Role of the potassium-chloride cotransporter type 2 (KCC2) in balancing excitation in the mouse hippocampus

A Dissertation

Submitted in Partial Fulfilment of the Requirements for the Degree of

Doctor rerum naturalium (Dr. rer. nat.)

to the Department of Biology, Chemistry, Pharmacy

of Freie Universität Berlin

by

Egor Byvaltcev

Berlin, 2024

The presented study was conducted between February 2018 and May 2023 under the guidance of Prof. Dr. Ulf Strauss at Institute of Cell Biology and Neurobiology, Charité – Universitätsmedizin Berlin

1st reviewer: **Prof. Dr. Ulf Strauss**
Institut für Zell- und Neurobiologie
Charité - Universitätsmedizin Berlin

2nd reviewer: **Prof. Dr. Ursula Koch**
Institute für Biologie
Freie Universität Berlin

Date of defense: 08.02.2024

Acknowledgements

This thesis owes its existence to the immeasurable kindness and unwavering support of countless wonderful humans who have surrounded me throughout these years. No matter the scale of impact, I am deeply thankful for your invaluable help and advice.

I am sincerely grateful to my supervisor Prof. Dr. Ulf Strauss for expert guidance, empowering encouragement and inexhaustive patience. Thank you for navigating me through the uncharted territories of the unknown, reminding me what is truly important and how to deal with complexity of life!

I would like to thank Prof. Dr. Victor Tarabykin and Prof. Dr. Alexey Semyanov for granting me the invaluable and lifechanging opportunity to embark on this incredible scientific journey.

I extend my heartfelt thankfulness to our wonderful collaborators – Dr. Thomas Gensch, Prof. Dr. Susanne Schreiber, Dr. Jan-Hendrik Schleimer and Mahraz Behbood – for their invaluable feedback, fruitful collaboration, and unyielding persistence.

I would also like to express my deepest gratitude to Dr. Ekaterina Epifanova, Dr. Ekaterina Borisova, Dr. Svetlana Tutukova, Dr. Alexandra Rusanova and Dr. Valentina Salina for their advice and expertise, providing priceless workarounds and shortcuts.

This work would not have been possible without my incredible lab teammates. Janna, Julia, Rike, Noah, Gabriel, Alice – thank you for your constant readiness to lend a hand and assistance! It has been an absolute honour and a stroke of luck to have had the opportunity to work alongside someone as exceptional as you!

Mark, Misha, Valera, Romash, Vitalya – thank you for GBs of memes and always keeping me smile regardless of distance and situation!

And last but certainly not the least, thank you Nastya for being there for me and going through the whole thing together. These years would have been unimaginably harder without you!

Declaration of Independence

Herewith I certify that I have independently prepared and written this thesis titled: “Role of the potassium-chloride cotransporter type 2 (KCC2) in balancing excitation in the mouse hippocampus”, and that I have not used any sources and aids other than those indicated by me. I also declare that I have not submitted the dissertation in this or any other form to any other institution as a dissertation.

_____ _____

Date Signature

Table of contents

Summary

In this study, I have investigated whether and how potassium-chloride cotransporter 2 (KCC2) influences extracellular potassium ($[K^+]_o$) levels during physiological synaptic activity in the mouse hippocampus. I have shown that KCC2 plays a crucial role in clearing excess $[K^+]_o$ in the vicinity of synapses during neuronal activity by temporarily reversing its mode of operation and transporting K^+ from extracellular space into spine. By manipulating KCC2 activity, I have observed changes in $[K^+]_o$ clearance, impacting neuronal excitability and synaptic transmission.

When KCC2 was blocked, there was an increase in $[K^+]_o$ levels around synapses, affecting astrocytic and neuronal responses and leading to enhanced excitatory signals. Conversely, enhancing KCC2 function reduced perisynaptic $[K^+]_o$, decreasing astrocytic response and lowering the frequency of excitatory signals. I have also shown that these effects were activity dependent and were more pronounced when other mechanisms of $[K^+]_o$ buffering, such as astrocytic K_{ir} channels, were compromised. Additionally, my results suggest that KCC2 activity can determine the efficiency of synaptic plasticity.

These findings highlight the significance of KCC2 at dendritic spines in regulating $[K^+]_o$ levels during physiological synaptic activity and its potential impact on information processing and storage. This research adds to previous evidence of tight connection of KCC2 with excitation balance in the brain.

Zusammenfassung

In dieser Studie habe ich untersucht, ob und wie der Kalium-Chlorid-Cotransporter 2 (KCC2) die Konzentration des extrazellulären Kaliums ($[K^+]_o$) während physiologischer synaptischer Aktivität im Hippocampus der Maus beeinflusst. Ich habe gezeigt, dass KCC2 eine entscheidende Rolle bei der Wiederaufnahme von überschüssigem $[K^+]_o$ in der Nähe von exzitatorischen Synapsen während neuronaler Aktivität spielt, indem es vorübergehend seinen Betriebsmodus umkehrt und K^+ aus dem extrazellulären Raum in die Dornfortsätze neuronaler Dendriten transportiert. Nach Manipulation der KCC2-Aktivität habe ich Veränderungen in der $[K^+]_o$-Aufnahme beobachtet, die sich auf die neuronale Erregbarkeit und synaptische Übertragung auswirkten.

Wenn KCC2 blockiert wurde, gab es einen Anstieg der $[K^+]_o$ um die Synapsen, was astrozytäre und neuronale Reaktionen beeinflusste und zur Verstärkung erregender Signale führte. Umgekehrt reduzierte die Steigerung der KCC2-Funktion das perisynaptische $[K^+]_o$, verringerte die astrozytäre Reaktion und senkte die Häufigkeit erregender Signale. Ich habe auch gezeigt, dass diese Effekte von der exzitatorschen Aktivität abhängig und ausgeprägter waren, wenn andere Mechanismen der $[K^+]_o$-Pufferung, wie die astrozytären Kir-Kanäle, beeinträchtigt waren. Darüber hinaus legen meine Ergebnisse nahe, dass die KCC2-Aktivität die Effizienz der synaptischen Plastizität beeinflussen kann.

Diese Ergebnisse betonen die Bedeutung von KCC2 an dendritischen Dornfortsätzen bei der Regulation der $[K^+]_o$ während physiologischer synaptischer Aktivität und deren potenziellen Auswirkungen auf die Informationsverarbeitung und -speicherung. Diese Forschung erweitert frühere Erkenntnisse über die enge Verbindung von KCC2 mit dem Erregungsgleichgewicht zentralnervöser Netzwerke.

Abbreviations

AMPA — α-amino-3-hydroxy-5-methyl-4-isoxazolepropionic acid

ACSF — artificial cerebrospinal fluid

ATP — adenosine triphosphate

BMI — (-)-bicuculline methiodide

CCC — cation-chloride cotransporter

CBX — carbenoxolone

CNQX — 6-Cyano-7-nitroquinoxaline-2,3-dione

DAP-5 — d-(-)-2-Amino-5-phosphonopentanoic acid

DMSO — dimethylsulfoxide

EGTA — ethylene glycol-bis(2-aminoethylether)-N,N,N',N'-tetraacetic acid

EPSC — excitatory postsynaptic currents

ESC — extracellular space

FLIM — fluorescence-lifetime imaging microscopy

GABA — γ-aminobutyric acid

GTP — guanosine triphosphate

KCC2 — K-Cl cotransporter 2

LTP — long-term potantiation

MWT — Mann–Whitney test

MQAE — n-(ethoxycarbonylmethyl)-6-methoxyquinolinium bromide

NKCC1 — Na-K-Cl cotransporter 1

NMDA — n-methyl-d-aspartate

OSR1 — oxidative stress-responsive kinase 1

PAPs — peripheral astroglial processes

PTX — picrotoxin

pTT — paired Student’s t test

ROI — region of interest

SPAK — STE20/SPS1-related proline/alanine-rich kinase

TT — Student’s t test

TTX — tetrodotoxin

WNK1 — with-no-lysine kinase 1

WSR — Wilcoxon signed-rank test

1. Introduction

1.1 Potassium (K^+) balance in the extracellular space (ECS)

The ability to generate electrical signals and propagate them to either similar or different tissue type cells distinguish neurons from other cells. That is possible due to the interplay of physical properties and unique proteins of biological membranes and intra- and extracellular mediums of the neuron and its surrounding ECS. Dynamic balance of ions across membranes and neuronal excitability are closely associated. ECS acts as a reservoir for ions and molecules that are necessary for creating and sustaining membrane potentials, chemical communications between cells and serves as a conduit of various complex metabolites (Syková and Nicholson, 2008).

A large portion of neurons' complex protein machinery is devoted to creating, maintaining, and restoring the membrane potential, which is derived from difference in ion concentrations across the membrane. Various homeostasis- and function-related processes deteriorate an existing gradient by changing membrane conductance and allowing ions to equilibrate. Synaptic transmission and following generation of action potentials cause transient but drastic changes in membrane potential and, hence, in the concentration gradient of ions. One of the earliest consequences recorded during brain activity was the increase of extracellular K^+ ion concentration ($[K^+]_o$) in the tissue.

ECS is usually described by two values: volume fraction α and diffusion permeability θ. α (defined as $\alpha = V_{ECS}/V_{tissue}$) represents the ratio of ECS to overall tissue volume and is tightly connected with concentration – in this case, α determines resilience to $[K^+]_o$ elevation. The smaller the α, i.e. the smaller the ECS volume, the larger $[K^+]_o$ can get after neuronal activity-derived K^+ extrusion. This is especially noticeable during pathological conditions and in synapse-rich regions of the brain such as cortex or hippocampus (Perez-Pinzon et al., 1995). θ (defined as $\theta = D_{ECS}/D_{agar,}$ where D_{ECS} and D_{agar} are diffusion coefficients measured in brain and in an approximation of free medium) shows diffusion velocity in a given medium compared to unrestricted diffusion. θ approaching 1 means diffusion velocity is close to the one in free and unconstraint medium.

Early data suggested that diffusion alone is not capable of sustaining adequate K^+ buffering capacity in ECS (Somjen, 1979). Conventional values of α and θ in averaged homogeneous brain regions are 0.2 and 0.4 respectively, meaning approximately 20% of the brain tissue is occupied by ECS and diffusion speed within this space equals to 40% of diffusion speed in free of any obstacles medium (Syková and Nicholson, 2008). Despite discrepancies between the layers in hippocampus, the same values were obtained for *stratum radiatum* (Hrabětová

et al., 2009; Saghyan et al., 2012). Another limiting factor of diffusion speed is the proteomic complexity of synaptic cleft and perisynaptic space (Loh et al., 2016). As shown for Ca^{2+} diffusion (Hrabětová et al., 2009) oppositely charged residues of membrane proteins or carbohydrates hinder free flow as well. Additionally, high tortuosity and dead-space microdomains further delay the diffusion (Syková and Nicholson, 2008). All these limitations are amplified if the region of interest (e.g. synaptic cleft, synaptic cluster etc.) instead of just neighbouring to one point source of excess K^+ is surrounded by multiple areas of elevated $[K^+]_o$.

Average $[K^+]_o$ in the ECS is kept at low vales around ≈ 2 - 3 mM. Early studies showed a possible range of K^+ fluctuations within 2 mM to 10 mM (Somjen 1979). Together with the nanoscopic size of space between cells in brain tissue, especially around synaptic clefts, even a relatively small rise of K^+ can have a considerate effect on $[K^+]_o$. Perturbations in $[K^+]_o$ may cause a variety of changes in neurons (as K^+ ions are ubiquitous in brain tissue and do not have specific receptors), such as shifts in resting membrane potential, altered synaptic signalling, augmented or suppressed activity of voltage-gated channels and other voltage- and gradient-dependent transporters (Kofuji and Newman, 2004). For instance, the synaptic activity-derived $[K^+]_o$ increase in the ECS had a biphasic effect on neuronal responses: modest electric stimulation of Schaffer collaterals augmented neuronal excitability, whereas strong and prolonged stimulation depressed axonal and postsynaptic responses (Poolos et al., 1987). According to the Goldman-Hodgkin-Katz equation, a mere increase in $[K^+]_o$ from 3 mM to 4 mM causes ≈ 2 mV depolarisation, and a further elevation to 10 mM depolarises membrane by ≈ 11mV. Therefore, precise and fine control of $[K^+]_o$ is crucial for maintaining adequate homeostasis and neuronal functioning.

The importance of $[K^+]_o$ changes in modulating cortical function and neural activity was demonstrated by *in vivo* recordings during different behavioural states (Rasmussen et al., 2019). Specifically, data revealed consistent increases in $[K^+]_o$ across the cortex (L2/3 and L5) when mice transitioned between stationary and locomotive states. Interestingly, the rise in $[K^+]_o$ levels produced multiplicative gain modulation in the visual cortex as well, enhancing responses to visual inputs. This supports the idea that K^+- mediated signalling might affect not only local synaptic population but can modulate cortex-wide baseline “state” and excitability.

Rise in local K^+ is, to a larger extent, dependent on postsynaptic NMDA receptors activation rather than AMPA receptors or K^+ release during axonal repolarization (Shih et al., 2013). This $[K^+]_o$ rise influences not only the resting membrane potential of locally situated neuronal and glial membranes but also facilitates Ca^{2+} entry to presynapses, which, in turn, further facilitates glutamate release and postsynaptic depolarisation (Geiger and Jonas, 2000). In this

way, postsynaptic NMDA-mediated K^+ release contributes to more glutamate release from presynaptic vesicles and K^+ ions act as a retrograde synaptic messenger (Shih et al., 2013). This sequence of events forms a positive feedback loop when each following excitation signal gets amplified by the previous, if excess K^+ is not removed from the surrounding ECS. Therefore, fast and efficient K^+ uptake is crucial for restraining such positive feedback loop during glutamatergic neurotransmission and several mechanisms of excess $[K^+]_o$ removal from the ECS is recruited.

In the hippocampus main $[K^+]_o$ restraining functions are carried out by Na^+/K^+-ATPase and astrocytes. The Na^+/K^+-ATPase is present in both neuronal and astrocytic membranes and is constantly active providing vital electrochemical gradients of Na^+ and K^+. While the Na^+/K^+-ATPase is an active transporter that depends on energy supply, the astrocytic membrane, especially in close vicinity of synapses, is enriched in K^+-inward rectifying channels (K_{ir}) that are highly sensitive to $[K^+]_o$ fluctuations, do not directly depend on ATP presence and serve to clear rapid K^+ elevations (Kofuji and Newman, 2004). In CA1 somatic patch-clamp recordings K_{ir}-derived astrocytic current is an easily identifiable long-lasting inward component that proceeds for seconds after artificial stimulation of axons. Parallel recordings of astrocytes and neurons revealed that astrocytic responses are reliable indicators of moderate to strong neuronal activity (Sibille et al., 2014).

Although astrocytic membrane is rich in several types of K_{ir} channels (Verkhratsky and Nedergaard, 2018), K_{ir}4.1 builds the channels that mediate the majority of K^+ uptake and tent to concentrate in astrocytic leaflets that surround synapses (Higashi et al., 2001). Knock-out of K_{ir}4.1 caused a depolarisation of astrocytes and compromised glutamate and K^+ uptake (Djukic et al., 2007). During intense neuronal activity, the depolarisation of astrocytic membrane decreases glutamate transporter kinetics and their capacity for glutamate clearance from the ECS. This suppressed absorption of glutamate results in elongated presence time of neurotransmitter within synaptic cleft and, as consequence, increased postsynaptic depolarisation caused by repeated activation of glutamatergic receptors (Tyurikova et al., 2022). Additionally, attenuated glutamate transporter efficiency results in impaired “isolation” of synapses and renders glutamate spillover more likely and frequent, which further contributes to excitation. This suggests that during intensified excitatory neuronal activity (e.g., strong activation of multiple synaptic clusters) the limited uptake resource is overwhelmed by both glutamate and K^+. Despite different kinetics of K_{ir}4.1 and glutamate transporters, these two processes will somewhat antagonise each other if glutamate release from presynapse persists for a long time.

To overcome K^+ accumulation, another astrocyte-mediated mechanism is employed. Excess K^+ from areas of elevated $[K^+]_o$ is being redistributed to areas with low/normal $[K^+]_o$ throughout the astrocytic syncytium via gap junctions (Kofuji and Newman, 2004). This process is also passive, i.e. does not depend on available ATP resources. Connexins are transmembrane proteins that form hemichannels with different permeability and when two hemichannels of neighbouring astrocytes interact they form a direct connection between these two astrocytes linking their cytoplasm. Cx43 and Cx30 are two main proteins that comprise gap junctions through which astrocytes can exchange ions and other low-mass molecules. Genetical suppression of these connexins resulted in impaired connectivity of the astrocytic syncytium, reduced capacity for $[K^+]_o$ clearance during synaptic activity and, thus, prolonged exposure to elevated $[K^+]_o$ and raised susceptibility to spontaneous epileptiform activity (Wallraff et al., 2006). Nevertheless, spatial buffering is efficient only if there is a "sink" for excess K^+ in a form of area with low/normal $[K^+]_o$. It is logically to suggest that in case of simultaneous activity of multiple presynaptic neurons there would be areas of neuropil surrounded by several areas with synaptic activation-derived elevated $[K^+]_o$ and there will be no "sink" for local astrocytes to dump excess K^+ to (except functioning blood vessels contact with which are limited).

Besides excitatory neurotransmission $[K^+]_o$ is affected by other channels and transporters such as: voltage-gated K^+ channels that repolarize neurons during action potentials, two-pore-domain K^+ channels and leak K^+ channels that participate in setting of the resting membrane potential (V_m), Na^+/K^+-ATPase being the main energy dependent transporter that creates the basis for V_m maintenance, Ca^{2+}-activated K^+ channels that are activated by Ca^{2+} entry during depolarisation, etc. This incomplete list includes different other types of proteins that take part in K^+ ionostasis. Yet, one particular family of transporters from this list has drawn much attention of research due to the simultaneous participation in the regulation of excitation and inhibition. This is the solute carrier family 12 (SLC12) that includes various transporters that transfer Na^+/K^+ and Cl^- ions across membranes.

1.2 The role of the neuronal K^+-Cl^- cotransporter KCC2 in neuronal excitation and inhibition

While K^+ concentration in the ECS is one of the main determinants in excitation, inhibition is mostly based on Cl^- ions and, more specifically, its internal concentration in neurons. Cl^--ionostasis determines the polarity and efficacy of GABA- and glycinergic transmission. In mature neurons, $[Cl^-]_i$ is kept at low levels rendering $GABA_A$ and glycine receptors hyperpolarising, i.e. allowing Cl^- to enter neurons upon activation. Besides ligand- and voltage-activated channels permeable to Cl^- there is a family of transporters that contribute to cellular

Cl^- ionostasis. This SLC12 family unites various cation-chloride cotransporters, including K^+-Cl^- cotransporters like KCC1, KCC2, KCC3, and KCC4, as well as Na^+-K^+-Cl^- cotransporters - NKCC1 and NKCC2, and an Na^+-Cl^- cotransporter. Among this list of transporters, particular interest in recent years is drawn to KCC2 as it is exclusively expressed in neurons, predominantly in somato-dendritic compartments and is a main contributor to Cl^- efflux (Kaila et al., 2014). It is also the only member of KCC that is not expressed in glia (Chamma et al., 2012).

KCC2 is a passive transporter, which means, it uses already stored energy in form of K^+ and Cl^- chemical gradients. In contrast to the Na^+/K^+-ATPase, KCC2 does not directly require energy for executing transport cycles. Each cycle of KCC2 operation results in transmembrane transfer of 1 K^+ and 1 Cl^- ion along the outwardly directed K^+ gradient (Payne, 1997). This characteristic determines electroneutrality of the co-transporter and explains absence of electrical current during its function. It is worth noting that, given normal conditions, constantly active KCC2 acts as another baseline source of $[K^+]_o$, however the majority of research has been focused on Cl^- extrusion by KCC2 (see below).

The KCC2 gene (*SLC12A5*) produces two distinct types of mRNA, KCC2a and KCC2b. The difference between KCC2a and KCC2b proteins lies in their N-terminal region. Specifically, KCC2a contains 40 unique amino acids, which include a potential binding sequence for the Ste20-related proline-alanine-rich kinase (SPAK) (Uvarov et al., 2007). In the neonatal mouse brain, KCC2a and KCC2b isoforms were found to have similar protein levels and distribution but in adult mice KCC2b was the prevalent form with KCC2a levels being much lower (Uvarov et al., 2009). Upregulation of KCC2 and increase in expression levels is paralleled with (and thought to be the main reason of) the hyperpolarising shift in E_{GABAA} (Rivera et al., 1999). A rise in the KCC2 associated Cl^- efflux lowers the baseline $[Cl^-]_i$ and reverses $GABA_A$ and glycine-mediated currents from inward (in immature neurons) to outward (in mature neurons).

Structurally, KCC2 consists of 12 transmembrane domains with 6 extracellular loops and intracellular N- and C-termini. These termini have multiple phosphorylation sites which, depending on their phosphorylation state, affect iontranslocaion function, ability to form homo- and heterooligomers (including other CCC family members) and anchor sites for interaction with cytoskeleton proteins (Blaesse et al., 2006; Heubl et al., 2017; Li et al., 2007; Simard et al., 2007; Uvarov et al., 2009). The functional KCC2 protein consists of disulfide-bonded homo-oligomers. This means that multiple KCC2 protein subunits must come together to form a functional transport-active unit. KCC2 oligomerization occurs throughout the nervous system and is age dependent. In immature neurons, KCC2 is primarily monomeric and transport inactive. As the nervous system matures, the monomer/oligomer ratio of KCC2 decreases,

indicating a shift towards more oligomeric and transport active KCC2 structures. Both forms of KCC2, i.e., transport-inactive and transport-active, are present at the plasma membrane (Blaesse et al., 2006).

Several reports showed that KCC2 distribution is non-uniform across CA1 pyramidal cells and is region- and/or layer-specific (Báldi et al., 2010; Gulyás et al., 2001). Báldi et.al. found that absolute values of surface density of KCC2 are higher in dendritic shafts than in spines, however, pointing out that rather high surface/volume ratio in spines contributes to efficacy of even smaller amount of KCC2 in maintaining low $[Cl^-]_i$ in spines. Gulyás et al. showed predominant colocalization of KCC2 and excitatory synaptic inputs. Interestingly, they also found that dendritic shafts contained low levels of KCC2, which is contrary to the results of Báldi et.al.

The tendency of KCC2 to localise in the vicinity of excitatory synapses where necessity of Cl^- extrusion is not obvious was started to be investigated by studies that focused on complete or partial suppression of the transporter. Experiments using KCC2-deficient cultured neurons showed a decreased malleability of actin filaments, which are essential for the morphogenesis, in dendritic spines. Deficient KCC2 decreases the motility of spines and, thus, impairs synaptogenesis (Llano et al., 2015). In other words, active and functioning KCC2 helps keeping spines more plastic and flexible and eases new spines formation. At the same time, KCC2-deficient neurons had elongated dendritic protrusions ranging from filopodia-like structures to protrusions with bulbous heads. That was not related to altered inhibitory signalling. A reduced number of functional excitatory synapses was also observed in these neurons. Interestingly, a nonfunctional KCC2 mutant that lack ion-transport function restored normal spine morphology, indicating independence of spine formation from K^+-Cl^- cotransport. The 4.1N protein was identified as potential interacting partner of KCC2, influencing spine development (Li et al., 2007). Such independence from active transport function was confirmed by premature transport-deficient KCC2 overexpression in developing pyramidal neurons (Fiumelli et al., 2013). Precocious KCC2 levels caused increased spine density and elevated spontaneous activity in layer 2/3 neurons. Notably, this effect is region specific as premature KCC2 expression in hippocampal neurons decreased spine density (Awad et al., 2018). While overall protein levels were similar between hippocampus and cortex (two similarly synapse-rich regions) a higher level of membrane-bound KCC2 was found in the hippocampus compared to the cortex at P7, but this difference disappeared by P20 (Awad et al., 2018). These findings indicate that functions of KCC2 extend beyond mere Cl^- extrusion as KCC2 affects spinogenesis and maintenance and even influences properties of excitatory transmission. These traits of the cotransporter, together with the previously mentioned

possible K^+ impact, suggest a larger impact and a more profound participation of KCC2 in balancing excitatory transmission.

Further confirmation on the close relation of KCC2 to excitatory neurotransmission came from analysis of KCC2 molecule trajectories in hippocampal neurons. Quantum-dot-based single particle tracking showed that KCC2 exhibited different behaviour near excitatory glutamatergic and inhibitory GABAergic synapses compared to extrasynaptic membrane regions (Chamma et al., 2012). Notably, at excitatory synapses KCC2 displayed reduced diffusion and increased confinement. This contrasted with its behaviour near inhibitory synapses, where KCC2 moved rather random resembling Brownian-type diffusion (Chamma et al., 2013; Heubl et al., 2017). Additionally, the analysis of synaptic dwell times revealed that KCC2 spent more time near excitatory synapses, suggesting a stronger anchoring to the scaffold in these areas. These findings collectively indicate that KCC2 specifically interacts with scaffolding molecules at excitatory synapses, leading to a diffusion-trapping mechanism at these locations but not at inhibitory sites, and that KCC2 overall tend to spend more time near/at excitatory synapses rather than inhibitory (Côme et al., 2020). More direct influence on excitatory transmission was revealed when suppressed KCC2 did not jeopardise spine functioning (suppression was implemented in mature neurons after spine formation) but hindered AMPA receptor stability and clustering in dendritic spines and decreased amplitude of mEPSC (Gauvain et al., 2011). Moreover, mere expression but not ion transport function of KCC2 was necessary for preventing AMPA-related changes in cells lacking KCC2 (Chevy et al., 2015).

All mentioned findings confirm that KCC2 affects various aspects of neuronal maturation and function, and this is not limited to its K^+/Cl^- transport function. Yet, at the same time, a lot of studies revealed that KCC2 itself is modified by changes in both excitatory and inhibitory transmission. Application of glutamate caused a sustained depolarization of E_{GABA}, shifting its equilibrium potential to more depolarized values. This shift in E_{GABA} was largely attributed to the loss of KCC2 function and decrease in the cell surface expression that was caused by dephosphorylation of KCC2 at C-termini residue S940, affecting its activity and membrane trafficking. Ca^{2+} influx was found to be involved in the glutamate-induced shift in E_{GABA}, and NMDA receptors played a crucial role in this process (Lee et al., 2011). It is worth noting, though, that in the mentioned study glutamate exposure lasted for minutes rather than seconds or milliseconds with a sustained concentration of 20 µM.

GABAergic transmission causes fluctuations of $[Cl^-]_i$ which also was found to up- or downregulate KCC2 activity. Specifically, $GABA_A$ receptor activation increased the confinement of KCC2 at the neuronal surface while blockade of these receptors increased mobility and membrane diffusion of KCC2 (Heubl et al., 2017). Thorough investigations

revealed that KCC2 activity is influenced by WNK1 which affected phosphorylation of T906/T1007 sites at the KCC2 C-terminal. Data showed that in immature neurons the majority of KCC2 is phosphorylated at T906/T1007 due to active WNK1. Suppressed WNK1 activity augmented KCC2-dependent Cl^- extrusion and shifted E_{GABA} to hyperpolarising values in immature neurons (Friedel et al., 2015).

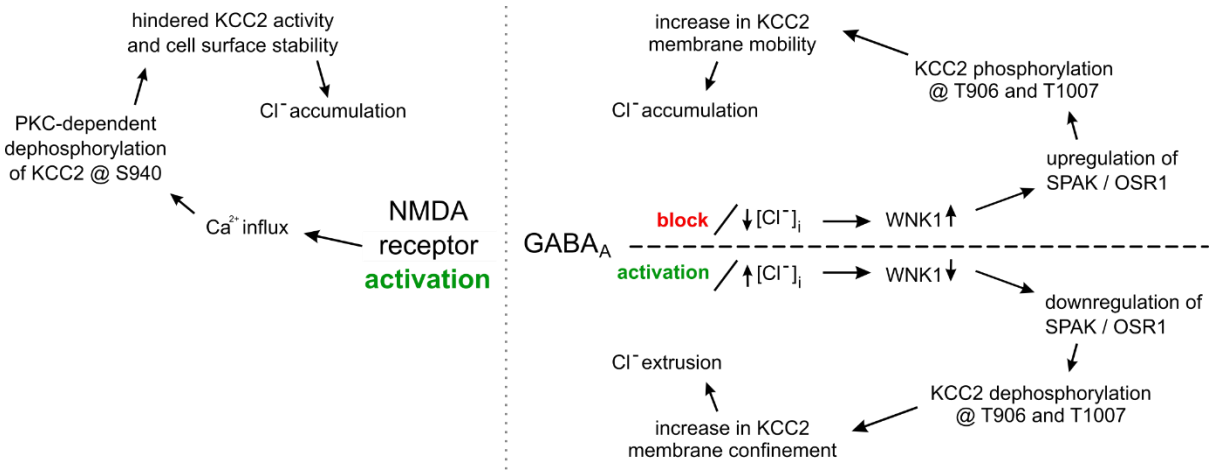

Figure 1. Schematic signalling pathways of NMDA-mediated (left) and $GABA_A$-mediated (right) KCC2 activity modulation.

In this way, rate and efficiency of Cl^- transport via KCC2 is at least partially affected by GABAergic transmission (Figure 1). Notably, WNK1 kinase counteracts low or high $[Cl^-]_i$ influencing not only KCC2 but by accompanying those effects with NKCC1 regulation as well. Downregulation of KCC2 and decrease in Cl^- extrusion rate goes in parallel with upregulation of NKCC1 activity which transports Cl^- into the neuron. Accordingly, in intact mature neurons under basal conditions majority of KCC2 is dephosphorylated at T906/T1007 which corresponds to higher confinement and lower membrane diffusion of KCC2 (Heubl et al., 2017; Rinehart et al., 2009). Additionally, KCC2 phosphorylation at T906/T1007 decreased the surface pool and increased the internalised pool of total KCC2 protein amount (Friedel et al., 2015).

It is worth noting though, all mentioned interactions that involve KCC2 are not direct and are mediated by complex signalling pathways, which include multiple proteins and messengers. Alteration of KCC2 might serve as a general signal to initiate several adaptive mechanisms to counteract or enhance perturbation. This complex network of signal-effect pathways highlights the crucial role of KCC2, and therefore K^+ and Cl^- transport, in the neuronal homeostasis and adaptation mechanisms to various physiological challenges.

1.3 Previous findings on KCC2 acting in reverse mode

As mentioned earlier, KCC2 uses energy stored in form of oppositely directed driving forces based on chemical gradients of Cl^- (inwardly directed) and K^+ (outwardly directed). Also, KCC2 transports ions in symport mode releasing both ions concurrently. The general possibility for KCC2 operation in both directions, extrusion and accumulation of ions, was demonstrated by wet experiments and mathematical modelling (DeFazio et al., 2000; Kakazu et al., 2000; Payne, 1997) (Table 1). These studies showed that the KCC2 transport mostly depends on $[K^+]_o$ and $[Cl^-]_i$ as changes in these values exert greater relative influence on driving forces. This property was confirmed by early experimental data (Jarolimek et al., 1999; Thompson and Gahwiler, 1989). In addition, experiments conducted by Jarolimek et al. (1999) showed that the extrusion capacity for Cl^- is more pronounced in dendritic compartments compared to the soma in cultured neurons. This might be explained by the surface/volume ratio, i. e. even a smaller absolute amount of transporter produces more pronounced effect due to the considerably smaller dendritic volume. This goes in line with reported discrepancies of KCC2 protein distribution throughout a given neuron (Báldi et al., 2010; Gulyás et al., 2001) and might explain detected somatodendritic gradient of $[Cl^-]_i$ and E_{GABA} (Jarolimek et al., 1999; Weilinger et al., 2022) (although, the experimental conditions were designed to mimic excitotoxicity (see Table 1)). This finding highlights the observation that KCC2-mediated transport has substantial impact on ionostasis, especially in areas with significant ions concentration fluctuations (synapses-rich dendritic compartment). Furthermore, the authors suggested that KCC2 reverse mode is not only possible but rather very likely under conditions when increased $[K^+]_o$ augments inwardly driving force of KCC2 (Jarolimek et al., 1999).

During naturally occurring processes and neuronal activity $[K^+]_o$ and $[Cl^-]_i$, that exert the most influence on KCC2 activity, can significantly fluctuate and even 1 mM change in either of them will cause substantial change in KCC2 driving force. For example, due to the narrow and limited ECS, simple movement-associated $[K^+]_o$ increase reached ≈ 1 mM (Rasmussen et al., 2019), and during intense excitation $[K^+]_o$ can reach 10-12 mM (Kofuji and Newman, 2004) which will greatly facilitate inward driving force for KCC2. Despite discrepancies in calculated absolute values, it is expected that in normal conditions KCC2 operates close to its thermodynamic equilibrium and ion transport reversal point lies within physiologically common concentrations of both $[K^+]_o$ and $[Cl^-]_i$ (DeFazio et al., 2000; Düsterwald et al., 2018; Payne, 1997).

Table 1.

Observations	Conditions	Reference
KCC2 basic properties characterisation using functional ^{86}Rb flux assay measurement.	KCC2 construct was transfected to HEK-293 cells, flux measurements at 24°C.	(Payne, 1997)
E_{GABA} depolarised after $[K^+]_o$ elevation. Furosemide (non-selective inhibitor of KCCs and NKCCs) reduced this depolarisation.	Patch-clamp recordings from 28-56 DIV cultured neurons at 22-25°C in HCO_3^- free medium. $[K^+]_o$ was elevated from 2 mM to 10 mM for ≈ 2 min (effect is noticeable after first 30 s).	(Jarolimek et al., 1999)
E_{GABA} depolarised after $[K^+]_o$ elevation. Furosemide abolished this depolarisation.	Patch-clamp recordings from P18-28 rat pyramidal neurons at 30°C. $[K^+]_o$ was elevated from 3.5 mM to 10 mM for ≈ 10 min.	(DeFazio et al., 2000)
I_{Gly} reversed from outward to inward and $[Cl^-]_i$ increased upon $[K^+]_o$ elevation.	Perforated patch from P13-15 rats at 22-26°C in HCO_3^- free medium. $[K^+]_o$ was elevated from 5 mM to 20 or 30 mM for ≈ 10 min.	(Kakazu et al., 2000)
NMDA-induced dendritic $[Cl^-]_i$ increase. Furosemide prevented this increase.	Patch-clamp + FLIM measurements from P25-38 rat 4/5 pyramidal neurons (slices) at 33°C. $[Cl^-]_i$ increased during increased V_H (+30 mV) and NMDA (20 µM) exposure for >10 min (effect is noticeable after first 5-7 min)	(Weilinger et al., 2022)

In NMDA-induced excitotoxic conditions KCC2 switches its transport direction to load neurons with K^+ and Cl^- leading to dendritic blebbing. Dendritic loading occurs through a coupling between NMDA receptors activation and Ca^{2+} entry, SK channel activation, $[K^+]_o$ accumulation, and KCC2 reverse mode at excitatory synapses (Weilinger et al., 2022). Remarkably, KCC2 can compensate for quite high artificial $[Cl^-]_i$ elevations. When neurons were whole-cell patched with $[Cl^-]_{pipette}$ = 80 mM, FLIM readouts from soma and dendrites revealed $[Cl^-]_i$ to stabilise near 40 mM and 20 mM respectively. This again points out that surface/volume ratio favours increased efficiency of K^+ and Cl^- extrusion by KCC2 in finer dendrites.

Enriched expression of KCC2 in the periphery of synapses and close interactions with spine-associated cytoskeleton as well as mutual interdependence on AMPA and NMDA receptors led to the assumption that KCC2 is also engaged in the balance of excitatory transmission via its ion transport function. Since KCC2 normally operates near its driving force equilibrium even a minor rise in $[K^+]_o$ might create conditions for reversing KCC2 ionic flux direction. Data on

$[K^+]_o$ fluctuations suggest that such elevations are not rare but rather likely. These expected oscillations were clearly observed by *in vivo* K^+-sensitive electrodes recordings (Rasmussen et al., 2019).

As KCC2 is located perisynaptically, it is subjected to pronounced amplitude oscillations of $[K^+]_o$. Near excitatory synapses, i.e. AMPA and NMDA receptors, local K^+ elevations are not only higher but persist for a longer time (Shih et al., 2013). This increases probability, driving force and duration of possible KCC2 reverse mode and, in connection with these parameters, total amount of transferred K^+ and Cl^- to a spine head. Given the chemical dependence of KCC2, such influx of ions will continue until the driving force of Cl^- grows strong enough to counteract the opposing driving force of the K^+ gradient. If and when this point is reached KCC2 will oscillate between import and export states bringing its net impact on ions concentration close to 0, although, since this state would be highly unstable as it requires constant and stable level of $[K^+]_o$. Assuming that in healthy tissue after physiological rise of neuronal activity (e.g., repetitive presynaptic bursts) the system returns to its baseline state with low levels of $[K^+]_o$, inwardly directed driving force will diminish and eventually return to its original values to favour K^+ export. Previously loaded to the spine excess, Cl^- will also contribute to outward driving force.

In this way, there could be a direct relationship between rate and direction of KCC2 and excitatory neurotransmission. The more intense and rapid the excitatory synaptic activity is, the more KCC2 transport is diminished and eventually forced to pump ions into a spine and in case of modest excitatory activity $[K^+]_o$ increase will not be high enough to flip driving force of KCC2 yet still be able to drop K^+ and Cl^- extrusion rate. Such neuronal activity dependence is frequently found across different mechanisms and, conveniently, also present in astrocytic current which was demonstrated to be highly sensitive to $[K^+]_o$ fluctuations (Dallérac et al., 2013; Ge and Duan, 2007).

1.4 Choice of experimental system

Hippocampal CA1 *stratum radiatum* represents a synapse-rich region mostly deprived of neuronal cell bodies and densely populated by astrocytes. This prevalence of synapses rather than cell bodies is advantageous for investigating synaptic activity related processes. Astrocytes penetrate neuropil volume with their fine peripheral astroglial processes (PAPs) and occupy individual non-overlapping domains. PAPs are closely associated with neuronal axons, spines and dendrites. In CA1 single astrocyte exclusively covers a volume of 66 000 μm^3 (Bushong et al., 2002) that on average contains up to ≈ 210 000 excitatory synapses, given 330 synapses per 100 μm^3 in non-fixed acute hippocampal slices (Kirov et al., 1999).

Although variable, the majority (70-80%) of spines within the astrocytic domain volume have direct contact with astrocytic membranes (Bernardinelli et al., 2014a; Gavrilov et al., 2018; Witcher et al., 2007). PAPs are very thin but at the same time represent up to 80% of cell total membrane, yet only 5 - 10 % of cellular volume (Reichenbach et al., 2010). Such intense intertwining of neurons and astrocytes and large membrane surface area is necessary for maintaining synaptic signal specificity, metabolite processing, neurotransmitter spillover control and ionic regulation – prerequisites of proper management of activity rich areas (Verkhratsky and Nedergaard, 2018).

Among other multiple essential functions of astrocytes, they are crucial players in keeping $[K^+]_o$ within the physiological range, both, in baseline and during increased excitatory activity conditions. A membrane highly permeable to K^+ renders astrocytes a main "gateway" in both long- and short-term $[K^+]_o$ control. In K^+ ionostasis related studies K^+-sensitive electrodes are commonly used to assess absolute values of $[K^+]_o$, which - given proper calibration - are quite accurate. It should be noted however, that ion-sensitive electrodes are unable to reflect fine and transient ion concentration due to a number of limitations: a) their slow kinetic is not suited for detecting events that are within action potential timescale, b) approximated sample area as pipette tip used for recordings is usually 2-3 µm wide and recorded area might contain both active and silent synapses, c) consequently the readout from electrode represent activity that "has left" synaptic clefts and underwent diffusion and dilution, d) inevitable unpredictable degree of mechanical perturbation causes somewhat blurred picture of structurally complex neuropil. Given that synaptic cleft is within tens of nm wide and average distance between neighbouring synapses is ≈ 500 nm (Rusakov and Kullmann, 1998) it is tempting to assume that K^+-sensitive electrode point more to a lower band of possible perisynaptic [K+]o values. Nevertheless, while alternative methods of monitoring $[K^+]_o$ are only starting to be implemented (Burgstaller et al., 2022), K^+-sensitive electrodes remain a reliable "industry standard" method in detecting changes in $[K^+]_o$.

Utilising extensive astrocytic coverage of synapses and PAPs' proximity to synapses may allow for faster and more sensitive signal registration by somatic patch-clamp compared to ion sensitive electrodes although with some trade-offs: a) since each astrocyte has unique morphology and arborization, uncontrollable surface area and overall "health" it is impossible to quantify absolute concentrations of K^+, b) low membrane input resistance attenuates actual elicited current in PAPs contributing to the signal losses c) compared to ion selective electrodes it is impossible to use the same "measuring device" with different slices and experimental setups making statistical inference less reliable. However, astrocytic patch-clamp has another great advantage. According to previous studies (Dallérac et al., 2013; Henneberger and Rusakov, 2012) astrocytic current is much faster than ion sensitive

electrodes which is of great importance when expected events have close to action potential temporal resolutions of tens to hundreds of ms.

Altogether, I hypothesised that during physiological excitatory synaptic activity the resulting abrupt and substantial $[K^+]_o$ elevation will shift the driving force of KCC2 and for a short period force it to flip transport direction from extrusion to intake which will be reflected by change in astrocytic current.

2. Methods

2.1 Animals

C57BL/6J 4 - 5 weeks old male mice were used for all experimental procedures. Animals were kept in groups of 3 - 5 individuals at 12 h day/night cycle at Charité central animal facility FEM (Berlin, Germany) with free access to water and food. All animals were healthy with no obvious behavioral changes, were not involved in previous studies, and were sacrificed during the light cycle. All procedures were performed in agreement with the European Communities Council Directive of September 22, 2010 (2010/63/EU) and carried out in accordance with state of Berlin rules (registration no. T0212/14).

2.2 Slice preparation

Mice were deeply anesthetized with isofluorane until breath frequency slowed down to 1-2 inhales per second. Before decapitation the tail reflex was checked (limb movements in response to tail tip squeeze) to ensure sufficient anaesthesia. After removing occipital and parietal bones, cerebellum was cut off and placed brain block containing hippocampus into cold (2 - 4°C) sucrose containing artificial cerebrospinal fluid (sucrose-ASCF). Time required for extraction of brain block after decapitation did not exceed 90 sec. Sucrose-ASCF contained (in mM): 85 NaCl, 50 sucrose, 26 $NaHCO_3$, 7 $MgCl_2$, 2.5 KCl, 1 NaH_2PO_4, 0.5 $CaCl_2$, and 10 glucose, pH = 7.4, osmolarity = 290 - 300 mOsm/l. Partial substitution of Na^+ with sucrose, low Ca^{2+} and high Mg^{2+} attenuate excitotoxicity as a consequence of mechanical injury derived damage of neurons and therewith prevent excess firing and Ca^{2+} loading. After ≈ 1 min incubation in sucrose-ASCF the brain block was placed in the cutting chamber of Leica VT1000S vibratome filled with cold (2 - 4°C) sucrose-ASCF. Coronal brain slices 300 µm thick were cut and placed into warm (34°C) sucrose-ASCF for recovery period of 30 minutes. After the recovery period slices were kept at room temperature (20 - 24°C) in HEPES-ASCF, which contained (in mM): 92 NaCl, 30 $NaHCO_3$, 20 HEPES, 5 Na-ascorbate, 2.5 KCl, 3 Na-pyruvate, 2 thiourea, 2 $MgSO_4$, 2 $CaCl_2$, 1.2 NaH_2PO_4*$2H_2O$, and 10 glucose, pH = 7.4, osmolarity = 290 - 300 mOsm/l. For experiments, slices were placed onto poly-l-lysine-covered (0.01%) 10 mm glass cover slips and then transferred to a submerged recording chamber mounted on an Olympus BX51WI microscope equipped with infra-red differential interference contrast microscopy and perfused with warm (34°C) ACSF at a rate of ~ 2 ml min^{-1}. ACSF contained (in mM): 119 NaCl, 26 $NaHCO_3$, 2.5 KCl, 2.5 $CaCl_2$, 1 NaH_2PO4, 1.3 $MgCl_2$ and 10 glucose, pH = 7.4, osmolarity = 290 - 300 mOsm/l. All solutions were constantly bubbled with carbogen (5% CO_2, 95% O_2) for maintaining pH ≈ 7.4 and saturating solutions with O_2. Solutions were

used for 3 days maximum after preparation including the day of preparation, were stored at 4°C in between experiments and never used more than once (discarded after use).

2.3 Electrophysiology

For eliciting synaptic activity extracellular bipolar tungsten or custom-made stimulating electrode was placed in CA1 *stratum radiatum* field of hippocampal slice. The stimulating electrode was custom-made from a glass pipette filled with ASCF (resistance of ≈ 50-100 kΩ) and two silver wires – one inside, the other wrapped to the outside of the pipette (Figure 2).

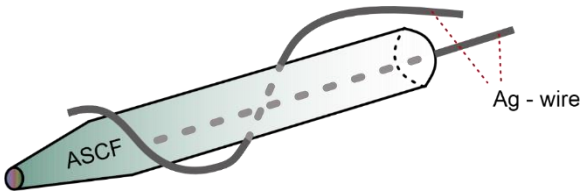

Figure 2. Schematic arrangement of custom-made stimulating electrode.

Each stimulation pulse had a rectangular shape and duration of 200 μs. Field excitatory postsynaptic potentials (fEPSPs) were recorded in CA1 *stratum radiatum* using glass pipettes with resistance of 1 to 2 MΩ filled with ACSF. Infrared differential interference contrast microscopy with Olympus 40XW water immersion was used for visual identification of astrocytes of CA1 *stratum radiatum* and neurons in CA1 *stratum pyramidale*. Cells 30 - 70 μm from slice surface (to minimize fraction of damaged membrane during slicing) and at least 250 - 300 μm from the stimulating electrode were used for experiments. Cells with barely visible membrane were considered for patch-clamp experiments, whereas cells with clearly visible and “wavy” membrane were omitted. Pipettes for neuronal somatic whole-cell patch-clamp experiments had resistance of 3 to 6 MΩ and contained (in mM): 128 potassium gluconate, 11 EGTA, 10 Hepes, 10 Na-phosphocreatine, 2 KCl, 2 Mg-ATP, 1 MgCl2, 1 CaCl2 and 0.3 GTP, (pH = 7.2, 297 - 303 mOsm/l). Pipettes for somatic whole-cell patch experiments of astrocytes had resistance of 3 to 6 MΩ when filled with (in mM): 105 potassium gluconate, 30 KCl, 10 Hepes, 10 Na-phosphocreatine, 4 Mg-ATP, 0.3 Na-GTP and 0.3 EGTA (pH 7.3, 280 mOsm/l). All glass pipettes were pulled with a Sutter Instruments P-97 puller.

Astrocytes in *stratum radiatum* were identified by small soma (5 - 10 μm), resting membrane potentials around –80 mV, low membrane resistance (6 - 15 MΩ) and passive membrane properties (linear I–V relation). After reaching the slice surface with patch-pipette, motions in X and Y axis were minimal to avoid mechanical damage, cell approaching was done swiftly to minimize exposure to intracellular solution (with high $[K^+]$). Astrocytes were clamped at –80

mV in voltage clamp mode and at 0 pA in current clamp mode, neurons were clamped at –70 mV in voltage clamp mode and 0 pA in current clamp mode. Experimental protocols were initiated at least 5 min after obtaining whole cell configuration to allow intracellular solution to equilibrate. Data was recorded with an EPC-10 USB double amplifier (HEKA, Lambrecht, Germany), digitized with sampling rate minimum of 10 kHz, stored using the PatchMaster software (HEKA, version 2x90) and analyzed using FitMaster (HEKA, version 2x90) and Origin2019 (OriginLab) software. Series or input resistance change of 20% or less was tolerated during one experiment otherwise recordings were excluded from statistical analysis.

K^+-sensitive electrodes were prepared as described earlier (Octeau et al., 2018). In brief, glass micropipettes were silanised, tip-filled with the K^+ ionophore cocktail (5% w/v valinomycin, 93% v/v 1,2-dimethyl-3-nitrobenzene, 2% w/v potassium tetrakis(4-chlorophenyl)borate) and backfilled with 10 mM HEPES buffered 300 mM NaCl. Before and at the end of each experimental day K^+-sensitive electrodes were calibrated and verified to have slope response at least 52 and no greater than 58 mV per log change in [K^+] with modified ACSF solutions containing 0.25, 2.5, 10 and 25 mM KCl (osmolarity was kept constant by respective increase or reduction of NaCl).

2.4 Morphology

In some experiments, astrocytes were filled with biocytin (0.1%, Invitrogen) and stained *post hoc*. In brief, slices were kept in 4% paraformaldehyde in 0.1% phosphate buffer (PB) (pH = 7.4) at room temperature for 1 h and then transferred to 0.1% PB at 4 °C. Prior to visualization, slices were washed 5 times in PB and incubated with fluorescent-conjugated streptavidin (Alexa Fluor-647, 1:1000, Invitrogen), in a PBS solution containing 3% normal goat serum, 0.1% TritonX-100, and 0.05% NaN3 for 48 h at 4°C. After incubation slices were washed in PB 5 times and mounted onto glass coverslips for further visualization. Counterstained astrocytes were imaged and identified using laser scanning confocal microscopy.

2.5 Fluorescence Lifetime Imaging Microscopy (FLIM)

Experiments have been performed using confocal one-photon and two-photon laser scanning microscope LSM 880 (Carl Zeiss, Jena, Germany) equipped with fs Ti:sapphire laser (Mai Tai HP (Spectra Physics, Milipitas, Ca, USA) operating at 80 MHz repetition rate. Average power incident on a sample was 5 mW. Prior to visualization slices were incubated in ASCF with 5 mM MQAE for 30 minutes at 34°C. Samples were excited at 750 nm and fluorescence signal was detected from 435 nm to 485 nm using band pass filter (460/50 BP, Chroma, Vt, US) and

short pass filter (690 SP, Chroma, US) with HPM-100-40 GaAsPhybrid detector (Becker & Hickl GmbH, Berlin, Germany) at NDD-port working in single photon counting mode. Single photon counting card SPC-150 (Becker & Hickl GmbH, Germany) was used to acquire photon statistics, which was further processed in SPCIMAGE 8.5 (Becker & Hickl GmbH, Germany).

2.6 Experiment design and reagents

Stimulation intensity was set to elicit ≈ 70 % of maximal astrocytic response to single stimulation pulse (≈ 0.2 – 0.6 mA). Schaffer collaterals were stimulated with 20 pulses 10 ms apart (referred as moderate stimulation). To minimize ongoing LTP, 2 preconditioning trains with 5 min interval were applied before proceeding with recordings and control trace was acquired 5 min after the 2nd preconditioning train (Figure 3).

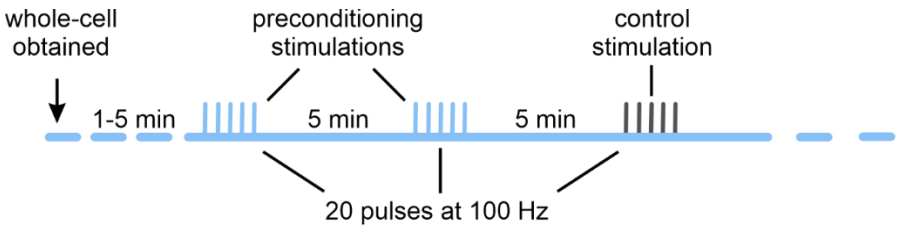

Figure 3. Schematic timeline of the pre-conditioning stimulation protocol.

For weaker synaptic activity 5 pulses 50 ms apart were applied (referred as weak stimulation) without prior preconditioning stimulation. For pressure ejection experiments a glass pipette containing (in mM): 91.5 NaCl, 30 KCl, 2.5 $CaCl_2$, 26 NaHCO3, 1 NaH_2PO_4, 1.3 $MgCl_2$ and 10 glucose was positioned 50 µm away and 10 - 20 µm above the soma of the patched astrocyte. Pressure ejection duration was 200 ms to mimic K^+ increase exposure time as with electrical stimulation. All experiments were performed in the presence of a $GABA_A$ antagonist, either (-)-Bicuculline methiodide (Tocris, Bristol, UK) (10 µM) or Picrotoxin (Tocris, Bristol, UK) (100 µM) and a cut was made between CA1 and CA3 to prevent the development of epileptiform activity.

KCC2 was blocked 10 µM VU0463271 (Tocris, Bristol, UK), based on its efficacy / reliability in brain slices (Delpire et al., 2012; Sivakumaran et al., 2015; Spoljaric et al., 2019) (dose dependence of VU0463271 approaches 100% at concentrations > 5 µM (Delpire et al., 2012). KCC2 was enhanced with 50 µM CLP257 (Tocris, Bristol, UK) or 10 µM closantel (Sigma-Aldrich, Steinheim, Germany). Glutamatergic excitatory transmission was blocked with 20 µM CNQX disodium salt (AMPA receptor blocker) (Tocris, Bristol, UK) and 25 µM DAP-5 (NMDA receptor blocker) (Tocris, Bristol, UK). $GABA_B$ receptors were blocked with 10 µM CGP54626

(Tocris, Bristol, UK). K^+ inward rectifying channels were blocked with 200 µM $BaCl_2$ (Sigma-Aldrich, Steinheim, Germany). Gap-junctions of astrocytes were disrupted by 100 µM carbenoxolone (CBX, Sigma-Aldrich, Steinheim, Germany) applied extracellularly or 25 µM when applied intracellularly. Perfusion time for VU0463271, CLP257, closantel and CGP54626 before gauging their effect was set to ≥ 12 min, for CNQX disodium salt, DAP-5 and $BaCl_2$ to ≥ 5 min, for CBX to ≥ 20 min (extracellular application) and ≥ 10 min (intracellular application). In LTP experiments potentiation was induced by Schaffer collateral stimulation with a single train (20 pulses at 100 Hz) without preconditioning stimulation.

2.7 Quantification and statistical analysis

Astrocytic peak current was searched for from at least 10 ms after the last stimulation pulse. Overall charge transfer was calculated as area under the curve with start at 10 ms after last stimulation pulse and end at cross point of recorded current and pre-stimulation mean resting membrane holding current (Figure 4). In experiments with CNQX and DAP-5 these values were gauged with 50 ms latency after the last stimulation pulse to completely exclude possible signal contamination by glutamate transporters current.

Figure 4. Example trace (20 s long recording) of CA1 astrocyte response in voltage-clamp mode to Schaffer collaterals stimulation with a single train of 20 pulses at 100 Hz. Stimulation artifacts were cut off. Note 10 ms interval from the last stimulation artifact before starting point of integral (Q). Peak I_{Kir} marked with red cross.

The Origin 2019 software was used for statistical analysis. A Shapiro-Wilk test was used to test for a normal distribution if n ≥ 7. In case of a normal distribution, paired Student's t test (pTT) was used and if a significant deviation from normal distribution occurred, the non-parametric Wilcoxon signed-rank test (WSR) was used. If n ≤ 6 WSR was used regardless of the normality test's result for paired samples. Results with $p < 0.05$ were regarded as statistically significant. Data are presented as mean ± standard error of the mean (SEM).

3. Results

For implementing the patch-clamp method, brain slices have several advantages: a) compared to *in vivo* conditions cells in brain slices are easily identifiable and accessible with recording and stimulating microelectrodes, b) unlike cell cultures, basic properties of cells and neuropil, given proper preparation and handling of slices, are left undamaged keeping initial connections and microstructure fairly intact, c) drugs administration is straightforward and reliable, d) electrical stimulation is more precise and controlled. Additionally, slices allow to access anatomically deep structures, which are difficult to reach in *in vivo* settings.

3.1 Astrocytic K_{ir} channel current is sensitive to activity dependent $[K^+]_o$ change

I chose hippocampal slices as a common model for investigations in neurobiology, focusing on the CA3-CA1 synaptic area — a microenvironment frequently studied in neurobiologial research — to investigate the potential KCC2 reverse mode during activity-dependent $[K^+]_o$ elevation. Axons of CA3 pyramidal neurons (Schaffer collaterals) are easily accessible for controlled artificial stimulation. These collaterals predominantly project to apical dendrites of CA1 pyramidal neurons forming glutamatergic synapses. Together with scattered interneurons and glial cells these axons form a synapse-rich hippocampal layer named *stratum radiatum*. Stimulation of Schaffer collaterals elicits glutamate release from presynaptic boutons, which triggers responses in CA1 pyramidal neurons. These responses can be easily and reliably gauged by patch-clamp recordings or by fEPSPs. By varying intensity, duration and pattern of stimulations it is possible to mimic neuronal activity of various strength.

Some of the Schaffer collaterals terminate on interneurons, which, in turn upon excitation, inhibit CA1 pyramidal neurons via GABAergic synapses in mature mice. $GABA_A$ receptors are permeable to Cl^- and, to a lesser extent, to HCO_3. As shown by previous research, both K^+ and Cl^- gradient determine the KCC2 driving force (DeFazio et al., 2000; Kakazu et al., 2000; Payne, 1997). Regardless of spatially different localization of excitatory (mostly spines) and inhibitory (mostly dendritic shafts and cell body) synaptic activation of GABA receptors might affect behaviour of KCC2 due to Cl^- diffusion from dendritic shafts to spines. To eliminate potential alteration of $[Cl^-]_i$, $GABA_A$ receptors were blocked by bicuculline methiodide (BMI, 10 µM) or picrotoxin (PTX, 100 µM) (see below) throughout all further experiments if not stated otherwise. To prevent epileptiform activity due to blocked inhibitory transmission a cut was made between CA3 and CA1.

I searched for astrocytes in the middle zone of CA1 *stratum radiatum* to ensure that the majority of given astrocytic domain is engaged during synaptic activity. After acquiring whole-cell configuration I verified that patched cells had typical astrocytic membrane properties — low membrane resistance (≈ 15 MΩ), depolarised resting membrane potential (≈ –85 mV), absence of action potentials and linear I-V dependence curve (Figure 5).

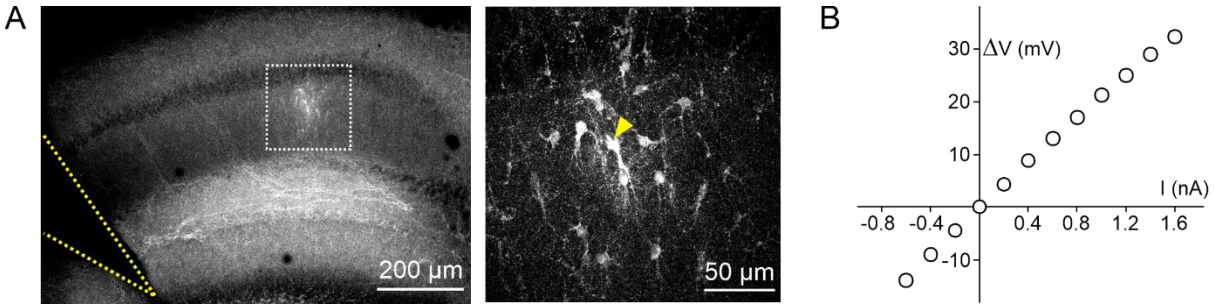

Figure 5. Typical locations of CA1 astrocyte used for experiments. **A** Left: Location of biocytin-labelled astrocyte syncytium in hippocampal CA1 *stratum radiatum*. Note the cut between CA3/CA1 (dotted yellow lines) to prevent hyperexcitability upon $GABA_A$ receptors block; right: close up on astrocyte syncytium (patched astrocyte indicated with yellow arrowhead). **B** Example of current-voltage relation of recorded astrocyte. Adapted from (Byvaltcev et al., 2023).

To mimic moderate synaptic activity, I used moderate stimulation of Schaffer collaterals with 20 pulses delivered at 100 Hz, which evoked substantial inward current in recorded astrocytes. In this current there were two clearly definable components – fast (occurring during and shortly after stimuli) and long-lasting (persistent for > 10 s). Notably, the peak of the long-lasting component did not overlap with the peak of the fast component, but was delayed on average by ≈ 198 ± 42 ms (n = 21) from the last stimulation artefact and had visibly slower kinetics. This overall behaviour was in line with previously reported astrocytic recordings consisting of fast glutamate transporters- and long lasting K_{ir}-channel mediated currents (Shih et al., 2013; Sibille et al., 2014).

To verify that the majority of recorded astrocytic response is suitable as measure of K^+ uptake I used Ba^{2+} (200 µM) to block K_{ir} channels (Alagem et al., 2001; Hibino et al., 2010). To exclude any impact of a Ba^{2+}-potentiated glutamate transporter current (Afzalov et al., 2013) I measured post-Ba^{2+}-treatment peak value of current at the same time point at which the peak current appeared in control trace (Figure 6). To minimise any contribution of glutamate transporter current I set the initial point for calculating integral at 10 ms after last stimulating pulse (Figure 6A). Resulting traces revealed an augmented glutamate transporter component

but, most importantly, the long-lasting component was drastically decreased (Figure 6B) both in amplitude and duration. This indicates that the astrocytic response to moderate stimulation of Schaffer collaterals mainly consists of K_{ir}-mediated K^+ uptake.

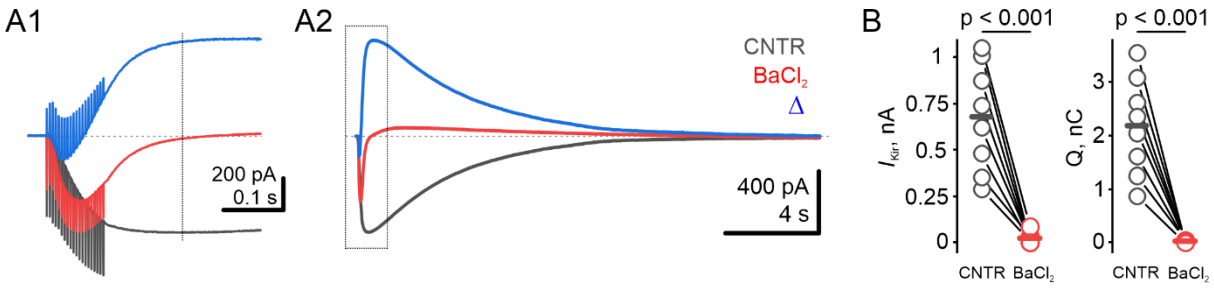

Figure 6. Recorded current was drastically reduced after application of $BaCl_2$ (200 µM) indicating a dominating fraction of K_{ir} channel-mediated current in the astrocytic response to Schaffer collateral stimulation. **A1** Close up of example traces (**A2**) before (*black*), after $BaCl_2$ application (*red*) and the difference between the two (*blue*). Vertical line indicates the time of peak I_{Kir} in the control trace and when corresponding value was measured under $BaCl_2$. **B** $BaCl_2$ nearly completely abolished K_{ir} channel-mediated currents ($I_{Kir\text{-}cntr}$ = 679 ± 103 pA, $I_{Kir\text{-}Ba}$ = 20 ± 10 pA, n = 8; Q_{cntr} = 2360 ± 303 pC, Q_{Ba} = 32 ± 7 pC, n = 7, pTT).

This allowed to assume that the peak current (further referred as peak I_{Kir}) and the integral (further referred as Q) of the astrocytic response are a suitable measure for the peak load of astrocytic K_{ir} channels and the total amount of transported ions or total charge transfer via K_{ir} channels respectively. Therefore, astrocytic recordings gauge the relative change of $[K^+]_o$ during neuronal activity in my setting (in line with previous studies (Meeks and Mennerick, 2007)).

3.2 Activity dependent changes of astrocytic response

Next, I checked if the peak I_{Kir} and Q during moderate stimulation is derived from postsynaptic activation as described earlier (Shih et al., 2013; Tyurikova et al., 2022). Since synapses of the *stratum radiatum* consist of CA1 dendrites and CA3 axons, K^+ ions may originate both from axonal action potentials and spine glutamate receptor activation. In the context of possible KCC2 reverse mode the origin of $[K^+]_o$ elevation is secondary. Nevertheless, if the majority of K^+ ions do not derive from postsynapses the $[K^+]_o$ elevation profile should follow axonal pattern and be evenly distributed along axons. In this case it would remain unclear why KCC2 is expressed in spines, and why astrocytic leaflets enwrapping synapses are enriched in K_{ir} channels. Another possibility, which will not contradict the distribution of KCC2 and K_{ir} channels, is that K^+ release sites are concentrated in presynaptic boutons. To investigate what

fraction of peak I_{Kir} and Q depends on postsynaptic activity, I washed in CNQX (25 µM) and DAP-5 (20 µM) – selective antagonists of AMPA and NMDA receptors, respectively. I added the blockers immediately after recording a control trace and set exposure time of blockers to 5 min after which I gauged the astrocytic response again. Resulting traces revealed a significant decrease of both, peak I_{Kir} and Q, after the same stimulation protocol (20 pulses at 100 Hz) (Figure 7). Approximately 75% of the initial peak I_{Kir} and Q was dependent on AMPA- and NMDA-activation. Combined with previous experiments with Ba^{2+}, this result suggests that astrocytic peak I_{Kir} and Q mostly depend on synaptic activity and can be used as reliable readout of glutamatergic receptor-related $[K^+]_o$ fluctuations.

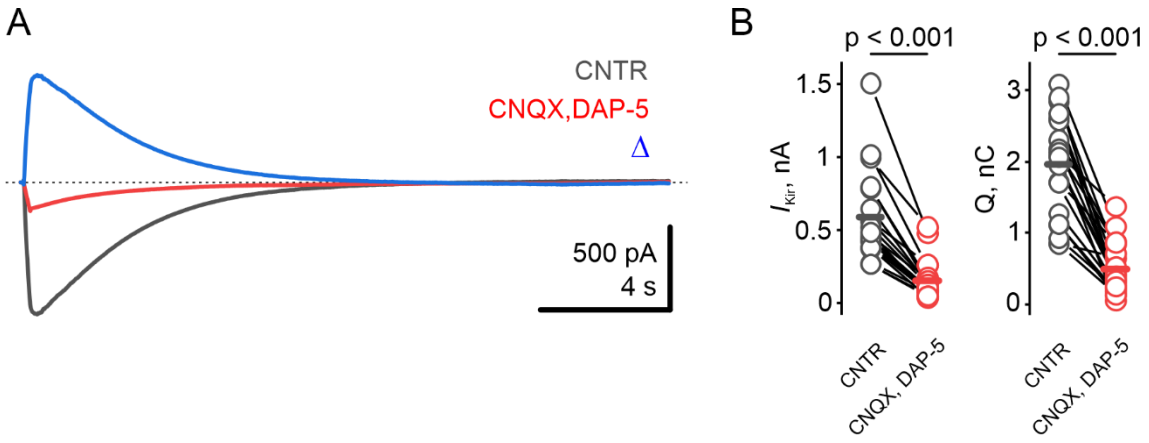

Figure 7. Peak I_{Kir} and Q depends on AMPA and NMDA receptor activation. **A** Example traces before (*black*), after CNQX (20 µM) and DAP-5 (25 µM) application (*red*) and the difference between the two (*blue*). To exclude glutamate transporters impact, measures of peak current and overall charge transfer were done at/starting from 50 ms after (indicated by vertical line) last stimulation artefact. **B** Approximately 75% of K_{ir} channel current is AMPA and NMDA receptor activation dependent ($I_{Kir\text{-}cntr}$ = 592 ± 66 pA, $I_{Kir\text{-}CNQX,DAP5}$ = 157 ± 28 pA, n = 21; Q_{cntr} = 1957 ± 154 pC, $Q_{CNQX,DAP5}$ = 495 ± 77 pC, n = 21, paired t-test).

Given that after blocking AMPA, NMDA and $GABA_A$ receptors there still was residual peak I_{Kir} and Q left, I questioned whether $GABA_B$ receptor activation might contribute to K^+ release. $GABA_B$ receptors previously were found to be tightly connected to various K^+ channels and K^+ ionostasis (Kaupmann et al., 1998; Sodickson and Bean, 1996; Wang and Lambert, 2000). First, I looked for any neuronal current that is detectable during stimulation under CNQX (25 µM) and DAP-5 (20 µM). Whole-cell recordings of CA1 neurons revealed a 1 - 1.5 s long outward current which was sensitive to CGP54626 (10 µM), a selective $GABA_B$ receptor antagonist (Figure 8A, B). Nonetheless, blocking $GABA_B$ receptors did not alter the astrocytic

response as indicated by unchanged peak I_{Kir} and Q (Figure 8C, D). In this way, $GABA_B$ receptor activation did not significantly contribute to astrocytic K^+ uptake under the current experimental conditions. It is worth noting that even if the $GABA_B$-receptor mediated impact on $[K^+]_o$ might be larger under more physiological conditions (absence of any blockers) it will further increase $[K^+]_o$ and therewith facilitate the KCC2 reverse probability.

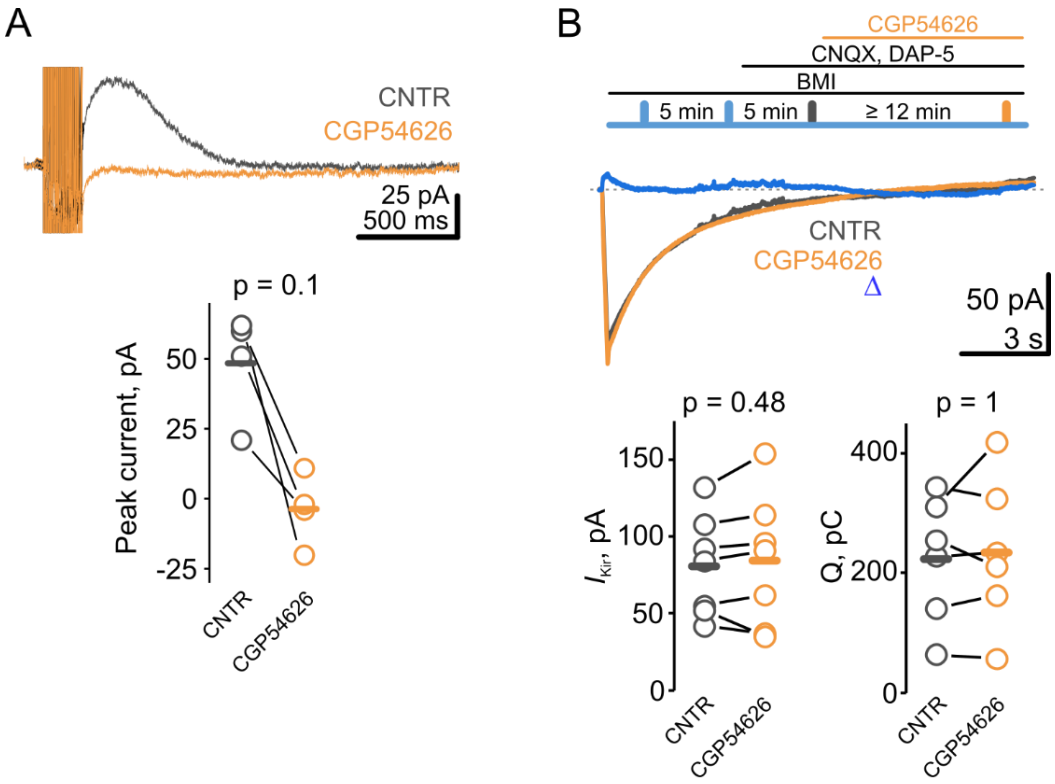

Figure 8. $GABA_B$ receptors did not contribute to the K_{ir} channel-mediated current. **A** Moderate stimulation in the presence of CNQX (20 µM) and DAP-5 (25 µM) (black) revealed an outward current in whole-cell recorded CA1 neurons that was abolished by the $GABA_B$ receptor blocker CGP54626 (orange) (peak $current_{cntr}$ = 45 ± 9 pA, peak $current_{CGP}$ = -4 ± 6 pA, n = 4, WSR). **B** $GABA_B$ receptor blocker did not alter peak I_{Kir} or Q ($I_{Kir\text{-}CNQX,DAP5}$ = 81 ± 12 pA, $I_{Kir\text{-}CNQX,DAP5,CGP}$ = 84 ± 16 pA, n = 7, pTT; $Q_{CNQX,DAP5}$ = 224 ± 43 pC, $Q_{CNQX,DAP5,CGP}$ = 235 ± 51, n = 6, WSR). Top: timeline of the experiment. Preconditioning stimulations were applied to exclude any LTP related changes in $GABA_B$ receptor activity and/or expression; middle: example traces of astrocytic recordings of control (*black*), with CGP54626 (*orange*) and the difference between the two (*blue*); bottom: population data on peak I_{Kir} and Q.

Another factor that might introduce ambiguity into further experiments is activity-dependent synaptic plasticity. The stimulation protocol used in aforementioned experiments (20 pulses at 100 Hz) is frequently used to elicit long-term potentiation (LTP) in hippocampal slices, although

the number of pulses used is often larger (≈ 50 - 100) (Henneberger et al., 2010; Zhu et al., 2015). This kind of synaptic facilitation inevitably will introduce a discrepancy in astrocytic responses due to augmented glutamatergic synaptic connection. To minimise such impact of LTP on possible treatment effects in future experiments, I preconditioned the slices with 2 trains of the same stimulation protocol before recording the actual control and treatment responses. This decision was based on the assumption that the capacity for increasing synaptic strength and LTP is limited within the relatively short timeframe of the planned experiments (10 - 20 min) and the contribution of each following stimulation to further enhancement of LTP will decrease. In other words, after a certain level of potentiation the limit of response increase is reached, and the system (CA3-CA1 synapses) becomes saturated and unsusceptible to further potentiation signals. To investigate this hypothesis, I recorded astrocytic responses in parallel with fEPSP in the *stratum radiatum* to monitor any change in excitatory transmission and compared traces from 3rd and 4th stimulation trains (Figure 9). While time intervals between first 3 trains was set to 5 min to allow time for potentiation development and saturation, interval between 3rd and 4th stimulation was set to at least 12 min to reveal any residual slowly developing gain in responses and to introduce a margin of time for chemical substance applications in further experiments.

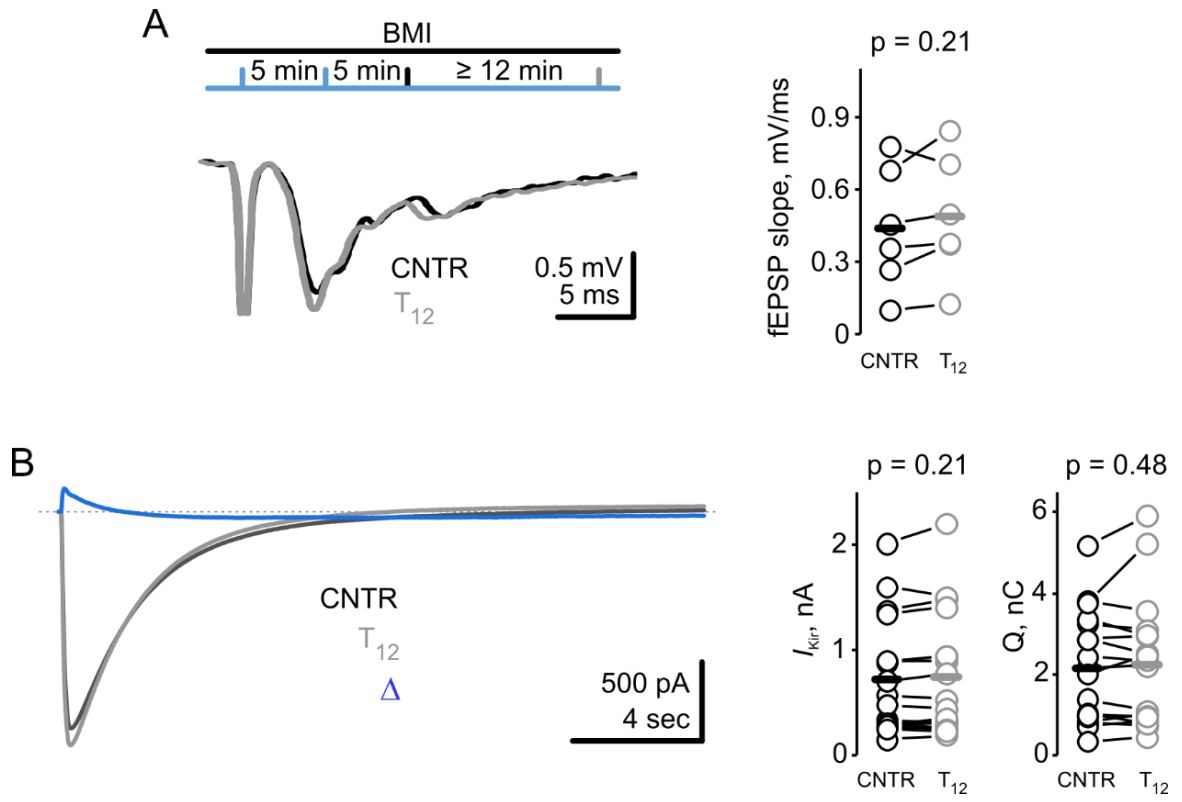

Figure 9. Preconditioning stimulation with 2 trains of 20 pulses at 100 Hz sufficiently “saturated” CA1 potentiating capacity. **A** There was no additional potentiation of fEPSP detected after preconditioning.

CA1 field responses were elicited by single pulse stimulation at 0.05 Hz. Traces were averaged for 3 min before control (CNTR, average of 9 traces) and T_{12} timepoint (T_{12}, average of 9 traces) and showed no change (fEPSP $slope_{cntr}$ = 0.438 ± 0.104 mV/ms, fEPSP $slope_{T12}$ = 0.486 ± 0.104 mV/ms, n = 6, WSR). Left top: timeline of the experiment; left bottom: example traces of fEPSP in control (*black*), at T_{12} (*grey*); right: population data on fEPSP slopes. **B** Following preconditioning peak I_{Kir} and Q remained unchanged ($I_{Kir\text{-}cntr}$ = 718 ± 128 pA, $I_{Kir\text{-}T12}$ = 739 ± 136 pA, n = 18; Q_{cntr} = 2156 ±322 pC, Q_{T12} = 2231 ± 369 pC; pTT) and unaffected by physiological and morphological LTP-derived changes. Left: example traces of control (*black*), at T_{12} (*grey*) and the difference between the two (*blue*); right: population data on peak I_{Kir} and Q.

Comparison of acquired traces did not show any significant difference in peak I_{Kir} and Q as well as in fEPSP slopes indicating similar amount of feedback between 3rd and 4th traces. Accordingly, 2 preconditioning stimulations are sufficient to saturate the potentiation capacity and diminish LTP interference well enough to enable further comparison of treatment effects. Additionally, this protocol allowed to exclude any significant influence of inevitable activity dependent morphological changes both in neurons and astrocytes (Bernardinelli et al., 2014b; Henneberger et al., 2020; Yuste and Bonhoeffer, 2001).

In this way, a substantial part of peak I_{Kir} and Q, and therefore of $[K^+]_o$, relies on AMPA and NMDA receptors activation and is not affected by $GABA_B$-associated K^+ release. Together with preconditioning this allowed for more precise comparison in subsequent experiments and reducing interference from activity-dependent alterations.

3.3 KCC2 attenuates postsynaptically released K^+

Next, I used this experimental protocol to find out what effect the block of KCC2 will have on astrocytic peak I_{Kir} and Q. To get auxiliary data I additionally recorded data from K^+-sensitive electrode in parallel with the astrocytic patch-clamp recording. The K^+-sensitive electrode was positioned approximately at the same distance from the stimulating electrode as the recorded astrocyte. Resulting traces showed increased astrocytic peak I_{Kir} and Q and an augmented signal from K^+-sensitive electrode (Figure 10). After I added the KCC2 blocker VU0463271 (10 µM) to the perfusion solution peak I_{Kir} increased on average by ≈ 26%, Q by ≈ 31% and K+-sensitive electrode signal by ≈ 10%. These results demonstrated that during moderate synaptic activity a deactivated KCC2 caused increased K^+ peak load and a larger total amount of charge transfer via K_{ir} channels in astrocytes. In parallel, K^+-sensitive electrodes showed an increased maximum $[K^+]_o$ as well but traces exhibited not only smaller value of change but also slower kinetics. Peak current was delayed by about 2 s compared to astrocytic traces

(both peaks are indicated by dotted line in Figure 10B). This deviation was likely caused by method-related limitations of the K^+-sensitive electrode recordings (see Introduction section 1.4). Additionally, astrocytic leaflets are closer to the synaptic cleft and the whole sampling area (astrocytic domain in neuropil) is larger. Regardless of quantitative differences both methods showed qualitatively similar results – active KCC2 is decreasing the amount of K^+ in the ECS during moderate excitatory transmission.

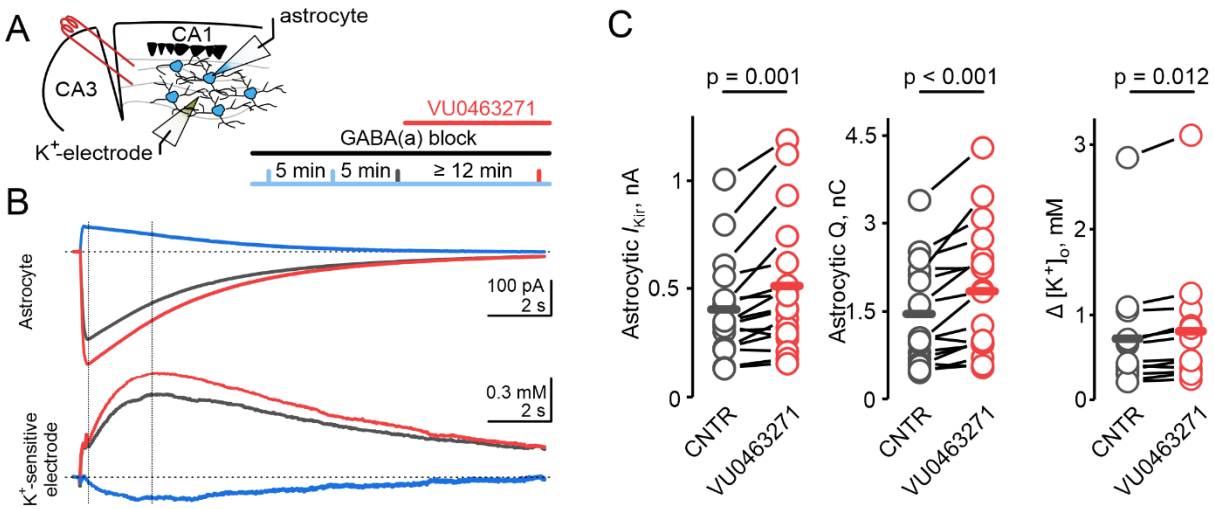

Figure 10. KCC2 inhibition increases transient $[K^+]_o$ elevation elicited by synaptic CA1 excitation. **A** Experiment scheme (top left) and timeline (bottom right). **B** Example traces of parallel astrocyte (top) and K^+-sensitive electrode (bottom) recording in control (*black*), with VU0463271 (*red*) and the difference between the two (*blue*). Vertical lines indicate peak currents of astrocytic (left) and K^+-sensitive electrode (right) recordings. Note peak current delay of the K^+-sensitive electrode compared to the astrocytic recording. **C** The specific KCC2 blocker VU0463271 (10 µM) increased astrocytic K_{ir} channels-mediated K^+-uptake by ≈ 30% ($I_{Kir\text{-}ctrl}$ = 405 ± 56 pA to $I_{Kir\text{-}VU}$ = 512 ± 77 pA; n = 17, WSR; Q_{cntr} = 1,443 ± 212 pC, Q_{VU} = 1,893 ± 270 pC, n = 17, pTT) as well as K^+-sensitive electrode peak voltage by ≈ 10 % (V_{cntr} = 5.8 ± 1.3 mV to V_{VU} = 6.4 ± 1.3 mV, n = 13, WSR) and respective Δ $[K^+]_o$ (Δ $[K^+]_{o\text{-}cntr}$ = 0.72 ± 0.19 mM to Δ $[K^+]_{o\text{-}VU}$ = 0.8 ± 0.21 mM, WSR). Adapted from (Byvaltcev et al., 2023).

After getting experimental hints that KCC2 reduces K^+ in the ECS, I set out to check if acquired data is not confounded by other factors. So far, I have used BMI to block $GABA_A$ receptors activation to prevent $[Cl^-]_i$ oscillations that would influence the KCC2 driving force. BMI is a competitive antagonist which means that it can be replaced by GABA at binding sites of receptors. During moderate stimulation of Schaffer collaterals alongside glutamate there is a substantial GABA release (Vargas-Caballero et al., 2010) from activated interneurons of CA1. This rise in GABA concentration further increases the probability of GABA displacing BMI at

$GABA_A$ receptors. Additionally, this process is accompanied by postsynaptic membrane depolarisation that facilitates postsynaptic load with Cl^- due to the transiently expanded difference between E_{Cl} and V_m. Elevation of $[Cl^-]_i$ will shift equilibrium potential for Cl^- towards more positive values, and consequently, cause a depolarisation of resting V_m, which will result in greater excitability and, consequently, larger K^+ release during and following excitation. To address this possibility and exclude such positive feedback loop in some of the previous experiments I used the non-competitive $GABA_A$ receptor blocker PTX (100 µM) instead of BMI. PTX also blocks spontaneous $GABA_A$ receptor openings further minimising Cl^- entry into neurons. Analysis of peak I_{Kir} and Q change indicated a comparable increase of values regardless of which $GABA_A$ receptor blocker I used (Figure 11). This data showed sufficient BMI block of $GABA_A$ receptors to prevented significant Cl^- entry into neurons.

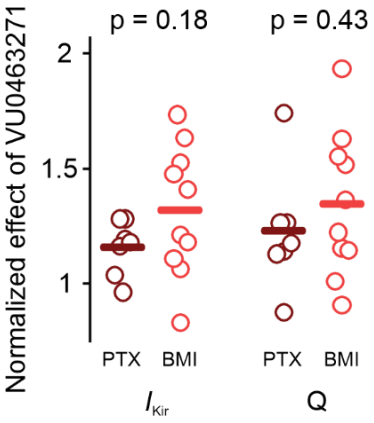

Figure 11. Normalized increase of astrocytic inward current under KCC2 block did not depend on the type of $GABA_A$ receptors blocker used to prevent concomitant $GABA_A$ activation and $[Cl^-]_i$ load of CA1 pyramidal neurons. VU0463271 comparably increased astrocytic whole-cell inward current following Schaffer collateral stimulation (20 pulses at 100 Hz) in the presence of $GABA_A$ receptor blockers PTX (100 µM) and BMI (10 µM) (I_{Kir}: PTX = 1.15 ± 0.04, n = 7; BMI = 1.31 ± 0.09, n = 10; Q: PTX = 1.23 ± 0.1, n = 7; BMI = 1.33 ± 0.1, n = 10; TT).

Another confounding factor that might cause misinterpretation of results from Figure 10 is the block of KCC2 itself. As mentioned, KCC2 is the major Cl^- extruder in mature neurons and its disfunction directly affects $[Cl^-]_i$. It is unclear, if the same connection is preserved when $GABA_A$ receptors are blocked and, if so, to what extent. Besides $GABA_A$ receptors there are multiple other ways for Cl^- to enter the cell (e.g. NKCC1, CICs, AEs etc.) (Rahmati et al., 2018). These proteins operate independently of KCC2 function and accumulate Cl^- inside neurons. But although being undoubtedly very important, KCC2 is not the only one protein that mediates export of Cl^- from a neuron. Other mechanisms (other KCCs, Na+-driven Cl^-/HCO^3 exchanger) might compensate or at least delay Cl^- accumulation when KCC2 is inactive (Alvarez-Leefmans, 2012). To find out if $[Cl^-]_i$ changed in CA1 neurons after KCC2 block we utilised fluorescence-lifetime imaging (FLIM). When $GABA_A$ receptors were blocked VU0463271 (10 µM) did not cause elevation of $[Cl^-]_i$ at least within the used experimental timeframe (Figure 12).

Altogether, experiments with PTX and data from FLIM measurements provide evidence for none or insignificant interference of neuronal $[Cl^-]_i$ fluctuations with peak I_{Kir}, Q and $[K^+]_o$ measurements.

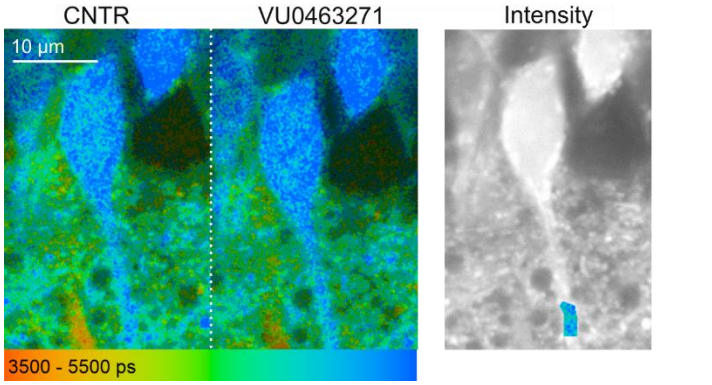

Figure 12. Blocking KCC2 did not change neuronal $[Cl^-]_i$. Left: Colour coded fluorescence lifetime images of CA1 loaded with the Cl^--sensitive dye MQAE without (left) and with VU0463271 (middle) and corresponding fluorescence intensity image with marked dendritic ROI (right), scale bar: 10 µm. Lifetime colour code scale bar: from 3500 ps (warm red, high $[Cl^-]_i$) to 5500 ps (cold blue, low $[Cl^-]_i$). Right: population data of ROI fluorescent lifetime without and with VU0463271 ($\tau_{ROI\ dendrite\ cntr}$ = 4.932 ± 0.040 ns vs. $\tau_{ROI\ dendrite\ VU}$ = 4.913 ± 0.028 ns, n = 22, pTT). Adapted from (Byvaltcev et al., 2023).

Another possible reason for the raised astrocytic K^+ uptake is an augmented neuronal excitability by VU0463271. Yet unreported, VU0463271 might modify channels or receptors and lead to an amplified response to excitation. If VU0463271 affected neuronal excitability in an activity independent way, this change could be detected by response to single evoked stimuli. To address this issue, I looked at fEPSP stability before and after adding the KCC2 blocker to the perfusion. I stimulated with single pulses at 0.05 Hz to avoid synaptic potentiation due to blocked $GABA_A$ receptors (Figure 13A). There was no significant potentiation detected neither in fEPSP slopes nor in fiber volleys conforming unchanged excitability of spines and axons respectively. Additionally, I checked if VU0463271 altered baseline spontaneous glutamatergic activity by assessing spontaneous EPSC characteristics of CA1 neurons before and after application of VU0463271 (Figure 13B). VU0463271 did not change presynaptic glutamate release probability (EPSC frequency) nor postsynaptic receptors (EPSC amplitude, rise time, decay time) and neuronal membrane properties (R_s, R_{in}). These results render side effects of VU0463271 on neuronal excitability unlikely and give additional indirect confirmation of unchanged $[Cl^-]_i$.

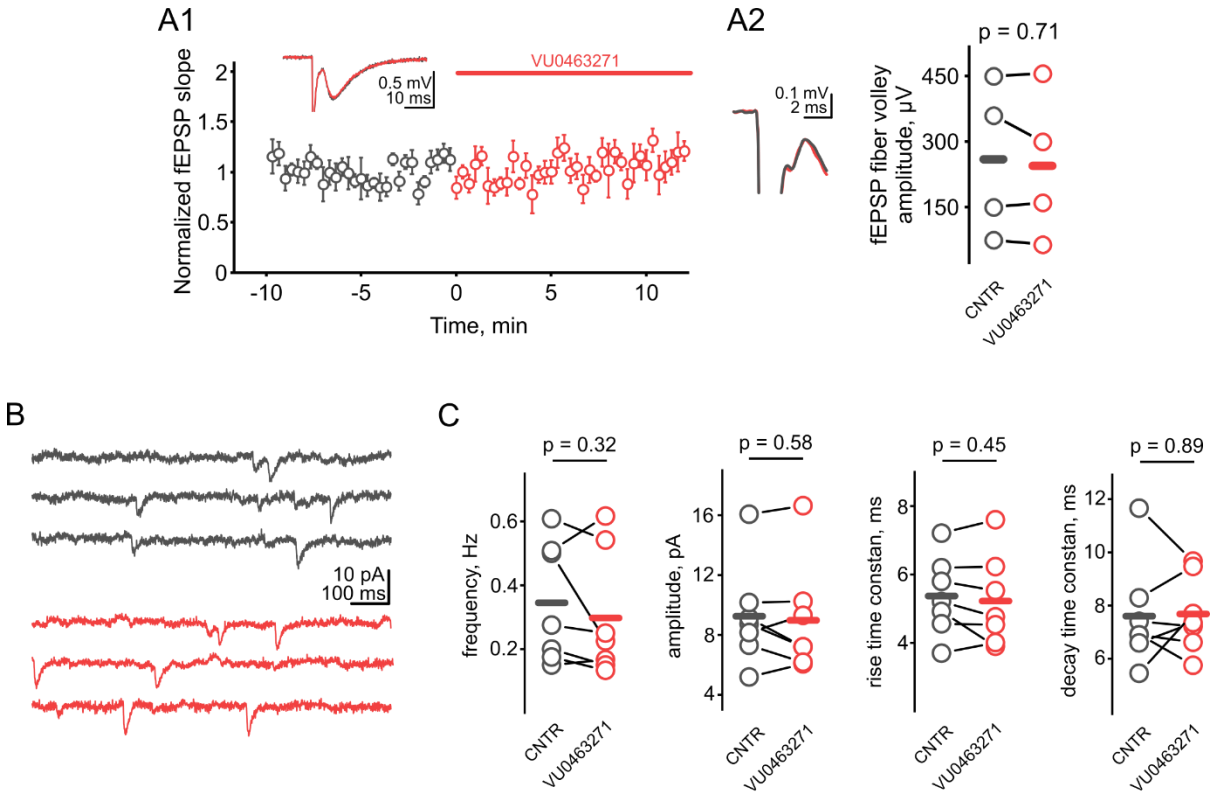

Figure 13. VU0463271 did not augment the excitability of CA3-CA1 synapses during $GABA_A$ receptor block**. A1** KCC2 block with VU0463271 (10 µM) left CA1 fEPSP slopes unchanged ($fEPSP_{cntr}$ = 1 ± 0.02, $fEPSP_{vu}$ = 1.03 ± 0.02, n = 7, p = 0.24, TT). Responses were elicited by single pulse stimulation of Schaffer collaterals at 0.05 Hz. Inset: averaged fEPSP traces before (*black*) and after VU0463271 (*red*). **A2** Fiber volley amplitudes of fEPSPs were not changed by VU0463271 as well (Amp_{cntr} = 259 ± 88 µV, Amp_{vu} = 245 ± 85 pV, n = 4, WSR). Together with **A1** this excludes an effect of VU0463271 on CA3 axons or synaptic transmission when KCC2 is not challenged. Note that a contribution of spontaneous spiking of CA3 pyramidal neurons is excluded by experimental setting, i.e. by the cut between CA3 and CA1 (Figure 5). **B** Excitability did not change within the CA1 associational network upon VU0463271 application as estimated by whole cell recordings of CA1 pyramidal neurons. Properties of spontaneous pharmacologically isolated (BMI, 10 µM) EPSCs (**C**) of CA1 pyramidal neurons voltage clamped at -70 mV (*black*) did not change under VU0463271 (*red*) (f_{cntr} = 0.35 ± 0.07 Hz, f_{vu} = 0.35 ± 0.07 Hz, n = 7; Amp_{cntr} = 9.24 ± 1.28 pA, Amp_{VU} = 8.97 ± 1.4 pA, n = 7; $\tau_{rise\text{-}cntr}$ = 5.37 ± 0.43 ms, $\tau_{rise\text{-}VU}$ = 5.22 ± 0.5 ms, n = 7; $\tau_{decay\text{-}cntr}$ = 7.60 ± 0.75 ms, $\tau_{decay\text{-}VU}$ = 7.68 ± 0.54 ms, n = 7; pTT; Rs_{cntr}/Rs_{VU}= 0.99 ± 0.03, n = 7, p = 0.84, TT).

Next, I asked if VU0463271 altered astrocytic K^+ uptake mechanisms. To rule out any K_{ir} channel related side effects of VU0432171 I recorded the astrocytic response to direct application of K^+ ions onto its surface via a pressure ejection pipette. To ease detection of any,

even minor, side effects of KCC2 I used a high concentration of K^+ for pressure ejection (30 mM). Additionally, I set the pressure ejection duration to 200 ms to make stimulation experiments (20 pulses at 100 Hz) and pressure ejection more uniform and mimic the same duration of K^+ release. As in this protocol I was interested in astrocytic response only to artificial K^+ elevation I did not preconditioned slices with electric stimulation. The Pressure ejection pipette was placed ≈ 50 µm from the cell body of patched astrocyte in attempt to engage K^+ uptake sites not only in cell's body vicinity, but also in endfeet. Resulting data indicated no significant difference between control and with VU0463271 (Figure 14). This renders VU0463271 (10 µM) interference with astrocytic K_{ir} channels' affinity and capacity of K^+ uptake unlikely and in addition hints that KCC2 that aggregate at spines did not contribute to clearing of elevated $[K^+]_o$ from "extrasynaptic" ECS.

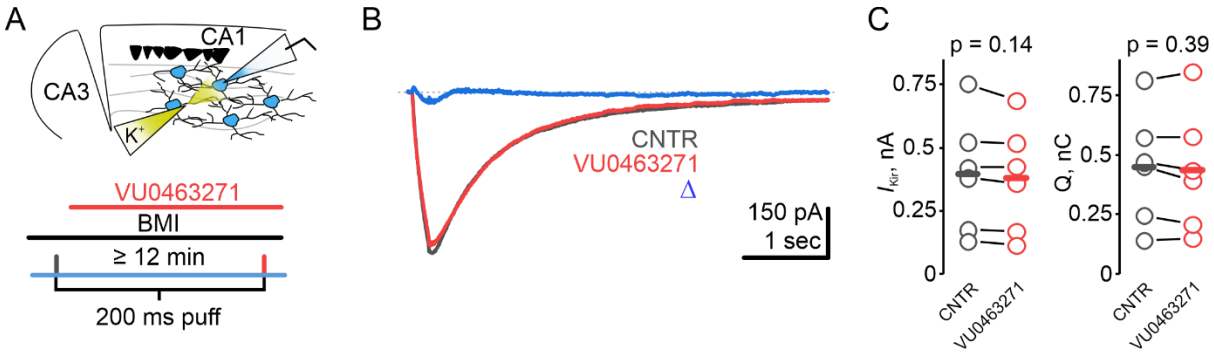

Figure 14. VU0463271 had no off-target effect on astrocytic membrane: The $[K^+]_o$ increase due to extracellular pressure injection was similar in time but differed in location compared to the spatially restricted perisynaptic $[K^+]_o$ increase upon synaptic stimulation. **A** Experiment scheme (top) and timeline (bottom). **B** Example traces before (*black*), after VU0463271 (10 µM) application (*red*) and the difference between the two (*blue*). **C** VU0463271 did not affect astrocytic peak I_{Kir} and Q in response to pressure ejection ACSF with increased K^+ (30 mM) onto astrocytic somata ($I_{Kir\text{-}cntr}$ = 396 ± 93 pA, $I_{Kir\text{-}VU}$ = 379 ± 87 pA, n = 6; Q_{cntr} = 448 ± 097 pC, Q_{VU}= 434 ± 107 pC, n = 6, WSR).

After this, I checked if any change in peak I_{Kir} and Q persists when glutamatergic transmission is blocked. As was shown before, around 75% of peak I_{Kir} and Q is dependent on AMPA and NMDA receptor activation, which triggers the majority of K^+ release during moderate synaptic activation. However, residual $[K^+]_o$ might be enough to cause temporal KCC2 reverse mode or at least bring KCC2 driving force close to 0. To find this out, I used the same stimulation protocol but with CNQX (20 µM) and DAP-5 (25 µM) during stimulation. After acquiring a control trace, I blocked KCC2 with VU0463271 (10 µM) but did not detect any significant changes neither in peak I_{Kir} nor in Q (Figure 15).

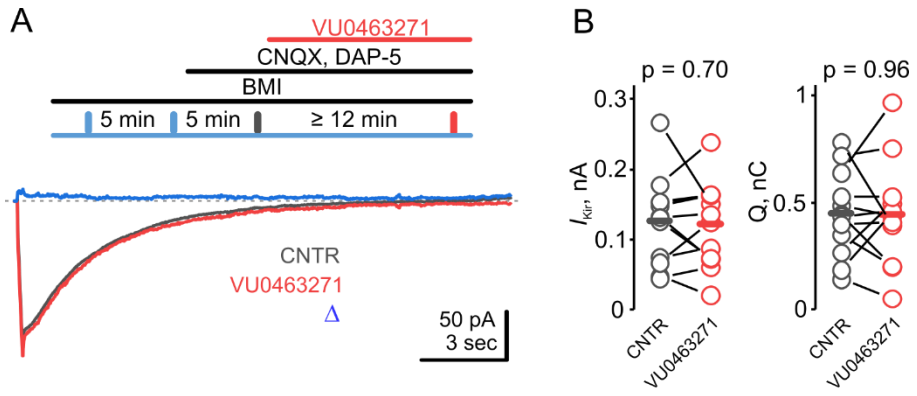

Figure 15. KCC2 reverse mode exclusively contributes to the clearance of $[K^+]_o$ elevations linked to glutamatergic synaptic activation. **A** Top: timeline of the experiment. Glutamate receptors were blocked after preconditioning stimulations to allow LTP; bottom: example traces under control conditions (*black*), with VU0463271 (*red*) and the difference between the two (*blue*). **B** After blocking NMDAR (DAP-5 25 µM) and AMPAR (CNQX 20 µM) the residual astrocytic peak I_{Kir} and Q are insensitive to KCC2 block (VU0463271 10 µM) ($I_{Kir\text{-}CNQX/DAP5}$ = 127 ± 18 pA, $I_{Kir\text{-}CNQX/DAP5/VU}$ = 122 ± 17 pA, n = 12; $Q_{CNQX/DAP5}$ = 449 ± 58 pC, $Q_{CNQX/DAP5/VU}$ = 446 ±71 nC, n = 12, pTT).

Artificial, as well as postsynaptic depolarisation independent $[K^+]_o$ increase, show a lack of sensitivity of peak I_{Kir} and Q to KCC2 flux, while moderate stimulation showed almost 30% increase of these values upon KCC2 block. From a first sight, these results seem to oppose each other since the former argues for no contribution of KCC2 and the later suggests substantial KCC2 participation in K^+ uptake. A likely explanation for this discrepancy is a combination of 2 factors: the amount of released K^+ and the temporospatial profile of such release. During moderate stimulation with intact AMPA and NMDA receptors K^+ release is distributed more evenly throughout the volume of the astrocytic domain (in comparison with focused pressure ejection) and is fairly simultaneous (neglecting temporal differences between opposing ends of astrocytic domain). Additionally, K^+ release is concentrated in/near synaptic clefts that are in the vicinity of astrocytic endfeet. In this way the astrocytic domain is somewhat enveloped and "permeated" by numerous point sources of K^+. In these conditions, $[K^+]_o$ might be elevated high enough and close enough to KCC2 localisation sites to cause its reverse mode.

Contrary to this, direct pressure ejection of even high $[K^+]$ is spatially limited and allows for spatial buffering process in recorded astrocyte. Moreover, during positive pressure ejection it is unclear if K^+ reaches targeted astrocytic endfeet in vicinity of synapses and not absorbed by and diluted on the way to them. Mechanical alteration of fine microstructure of neuropil is altered as well due to the pressure ejection itself to the slice. Meanwhile, in case of blocked

AMPA and NMDA receptors K^+ release is much lower, lacks synaptic cleft specificity and concentrated rather along stimulated axons. Nevertheless, there is also a possibility that during pressure ejection experiments and while AMPA and NMDA receptors were blocked KCC2 block effect was simply undetectable due to either the low “sensitivity” of astrocytic membrane or due to small impact of KCC2 block on peak I_{Kir} and Q in these conditions. In this way, experiments with electric stimulation during intact glutamatergic transmission supports the hypothesis that KCC2-mediated increase in astrocytic K^+ uptake requires a substantial amount of released K^+.

In a nutshell, my results suggest that blocking of the KCC2 leads to elevated $[K^+]_o$ during physiologically moderate synaptic activity, indicating that synaptic activity derived K^+ in the ECS can be reduced by reversed KCC2. I have validated the specificity of the observed effects by excluding potential confounding factors, such as $[Cl^-]_i$-dependent depolarisation or direct neuronal potentiation by KCC2.

3.4 Confounded astrocytic syncytium potentiates KCC2 contribution

To get more evidence of the close connection of KCC2 activity and astrocytic K^+ uptake, I investigated possible opposite effect of KCC2 potentiation on peak I_{Kir} and Q. In contrast to increasing peak I_{Kir} and Q with KCC2 blocked, facilitation of KCC2-mediated transport should reduce peak I_{Kir} and Q as more K^+ is captured by KCC2. Surprisingly, the KCC2 enhancer CLP257 (50 µM) did not cause any change in peak I_{Kir} and Q (Figure 16A). This chemical had been successfully used before (Ferando et al., 2016), although its efficiency was questioned by other studies (Cardarelli et al., 2017).

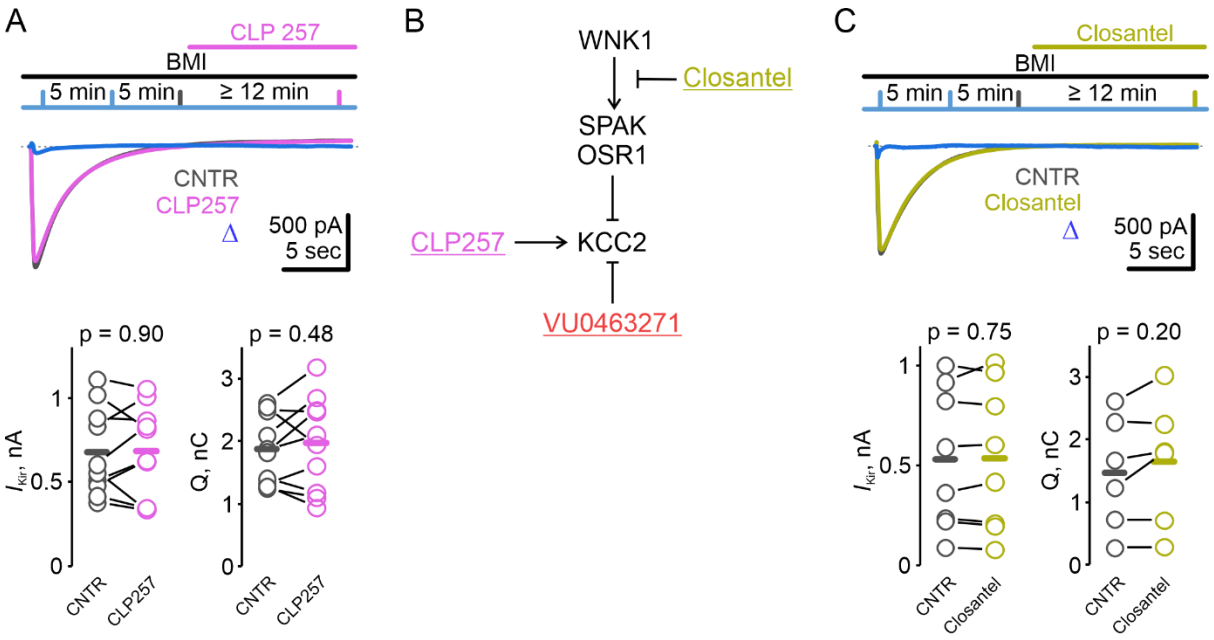

Figure 16. Direct (with CLP257) and indirect (with closantel) facilitation of KCC2 had no effect on peak I_{Kir} and Q. **A** KCC2 enhancer CLP257 (50 μM) did not alter astrocytic peak I_{Kir} and Q ($I_{Kir\text{-}cntr}$ = 680 ± 82 pA, $I_{Kir\text{-}CLP}$ = 685 ± 86pA; n = 10; Q_{cntr} = 1869 ± 173 pC, Q_{CLP} = 1970 ± 238 pC, n = 10, pTT). Top: timeline of the experiment; middle: example traces under control conditions (*black*), with CLP257 (*magenta*) and the difference between the two (*blue*); bottom: population data on peak I_{Kir} and Q. **B** Schematic mode of action for CLP257, VU0463271 and closantel. **C** The SPAK/OSR1 inhibitor (and therewith KCC2 enhancer) closantel (10 μM) did not change astrocytic response ($I_{Kir\text{-}cntr}$ = 532 ± 124 pA, $I_{Kir\text{-}Closantel}$ = 538 ± 129 pA; n = 8, pTT; Q_{cntr} = 1484 ±361 pC, $Q_{closantel}$ = 1717 ± 381 pC, n = 6, WSR). Top: timeline of the experiment; middle: example traces without (*black*) and with closantel (*gold*) and the difference between the two (*blue*); bottom: population data on peak I_{Kir} and Q. Adapted from (Byvaltcev et al., 2023).

Another way to boost KCC2 activity is to inhibit WNK1, which controls KCC2 phosphorylation at T906/T1007 (Friedel et al., 2015). WNK1 is involved in multiple crucial messaging cascades and its alteration might produce a broad range of uncontrollable effects in various neuronal functions. To limit concomitant effects, I used closantel (10 μM) which is a SPAK and OSR1 inhibitor (Figure 16B). The latter kinases facilitate KCC2 phosphorylation at T906/T1007 impeding KCC2 membrane stability. In this way, by diminishing SPAK and OSR1, closantel disinhibits KCC2. However, after closantel wash-in, as in the CLP257 case, astrocytic peak I_{Kir} and Q did not change (Figure 16). Such a lack of change in peak I_{Kir} and Q might be explained by a) improper choice of potentiating agents and/or chemicals, b) temporal limitations of potentiation (i.e. KCC2 requires larger exposure time to enhancers), c) low susceptibility of KCC2 to facilitation which implies that majority of KCC2 molecules are unable to increase transport rate and operating at already maximum rate.

Taking that previous use of CLP257 (Ferando et al., 2016) and closantel (Heubl et al., 2017) with comparable drug exposure times was effective I decided to test the assumption that KCC2 potentiation is difficult to reliably detect in given experimental conditions with the used methods. The astrocytic membrane has a very low input resistance causing substantial losses of current from distal parts of the cell. This leak also spreads to neighbouring astrocytes via connexins and might be up to 30% (Wallraff et al., 2006). In attempt to limit leak current and amplify the recorded signal during potentiation of KCC2, I used carbenoxolone (CBX, 100 µM) to block connexins and disrupt the astrocytic syncytium (Figure 17A). Also, blocked connexins prevent spatial buffering in astrocytes which further saturates the astrocytic uptake mechanisms and potentially increases $[K^+]_o$. Surprisingly, closantel attenuated both peak I_{Kir} and Q by about 15%, however, CLP257 still did not cause any decrease but opposite to expected – augmented peak I_{Kir} and Q (Figure 17B,C).

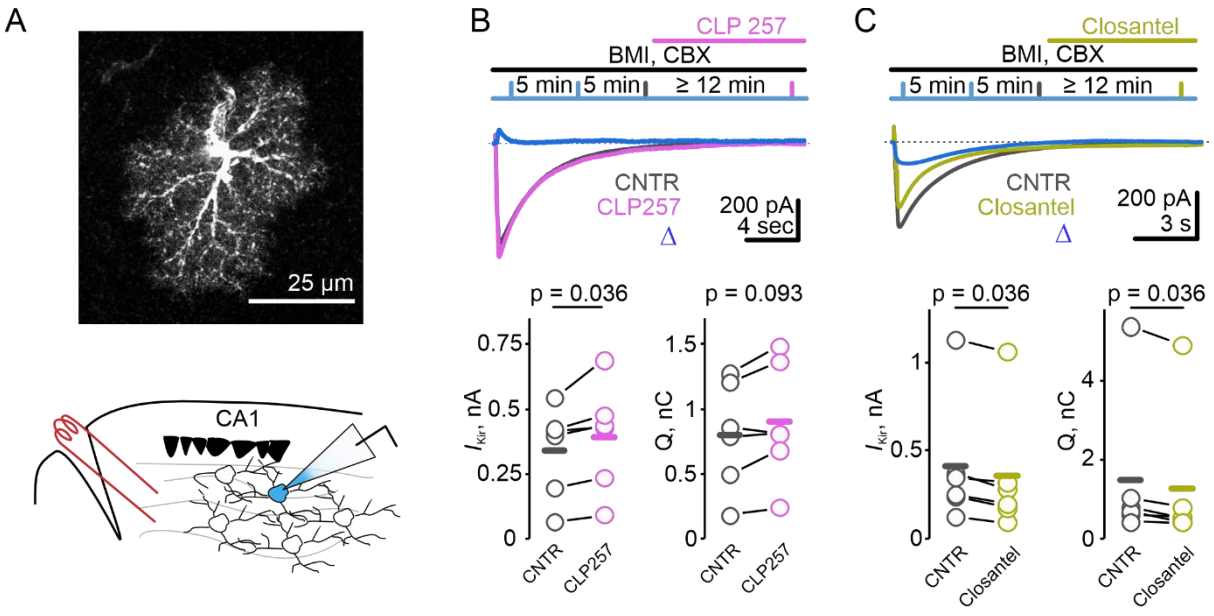

Figure 17. Disruption of the connexin-mediated connection between astrocytes revealed closantel- but not CLP257-mediated reduction of astrocytic response. **A** Top: Biocytin-labeled single *stratum radiatum* astrocyte isolated by the gap junction blocker CBX; scale bar: 25 mm. Bottom: experimental scheme. **B** Incubation with CBX (100 µM) increased astrocytic peak I_{Kir} but did not change Q ($I_{Kir\text{-}cntr}$ = 340± 72 pA, $I_{Kir\text{-}CLP}$ = 393 ± 84 pA; n = 6; Q_{cntr} = 801 ±170 pC, Q_{CLP} = 898 ±187 pC, n = 6, WSR). Top: timeline of the experiment; middle: example traces under control conditions (*black*), with CLP257 (*magenta*) and the difference between the two (*blue*); bottom: population data on peak I_{Kir} and Q. **C** Closantel (10 µM) decreased peak I_{Kir} and Q in the presence of CBX (100 µM) for > 20 min prior to recordings ($I_{Kir\text{-}ctrl}$ = 411 ± 148 pA, $I_{Kir\text{-}closantel}$ = 355 ± 144 pA; n = 6; Q_{cntr} = 1491 ± 779 pC, $Q_{closantel}$ = 1270 ± 727 pC, n = 6, WSR). Top: timeline of the experiment, middle: example traces without (*black*) and with closantel (*gold*)

traces and the difference between the two (*blue*); bottom: population data on peak I_{Kir} and Q. Adapted from (Byvaltcev et al., 2023).

CLP257 is reported to increase the surface expression of KCC2 (Gagnon et al., 2013) while closantel causes dephosphorylation of KCC2 at T907/T1007. Given the results above, KCC2 in dendritic spines might be more susceptible to augmentation via de-/phosphorylation process rather than surface protein level elevation. Regardless, detecting KCC2 potentiation required disrupting connections between astrocytes by blocking connexins and, even then, registered relative change was smaller than change during KCC2 block (≈15% and ≈30% respectively). This suggests that during the used experimental conditions KCC2 has a small capacity towards potentiation. To note, I have not tested for CLP257 effects during a longer timeframe that is putatively needed to increase total protein levels which is exposed to surface afterwards.

Since only closantel showed the expected decrease of peak I_{Kir} and Q, I checked possible side effects of closantel in conditions its presence had decreased peak I_{Kir} and Q (BMI and CBX in perfusion; as for VU0463271). Pressure ejection of ASCF with high $[K^+]_o$ onto the astrocyte or Schaffer collateral stimulation when AMPA and NMDA receptors were blocked did not change peak I_{Kir} and Q (Figure 18). This suggested that closantel did not hinder astrocytic K^+ uptake capacity, too, and only had a relevant impact during massive K^+ release.

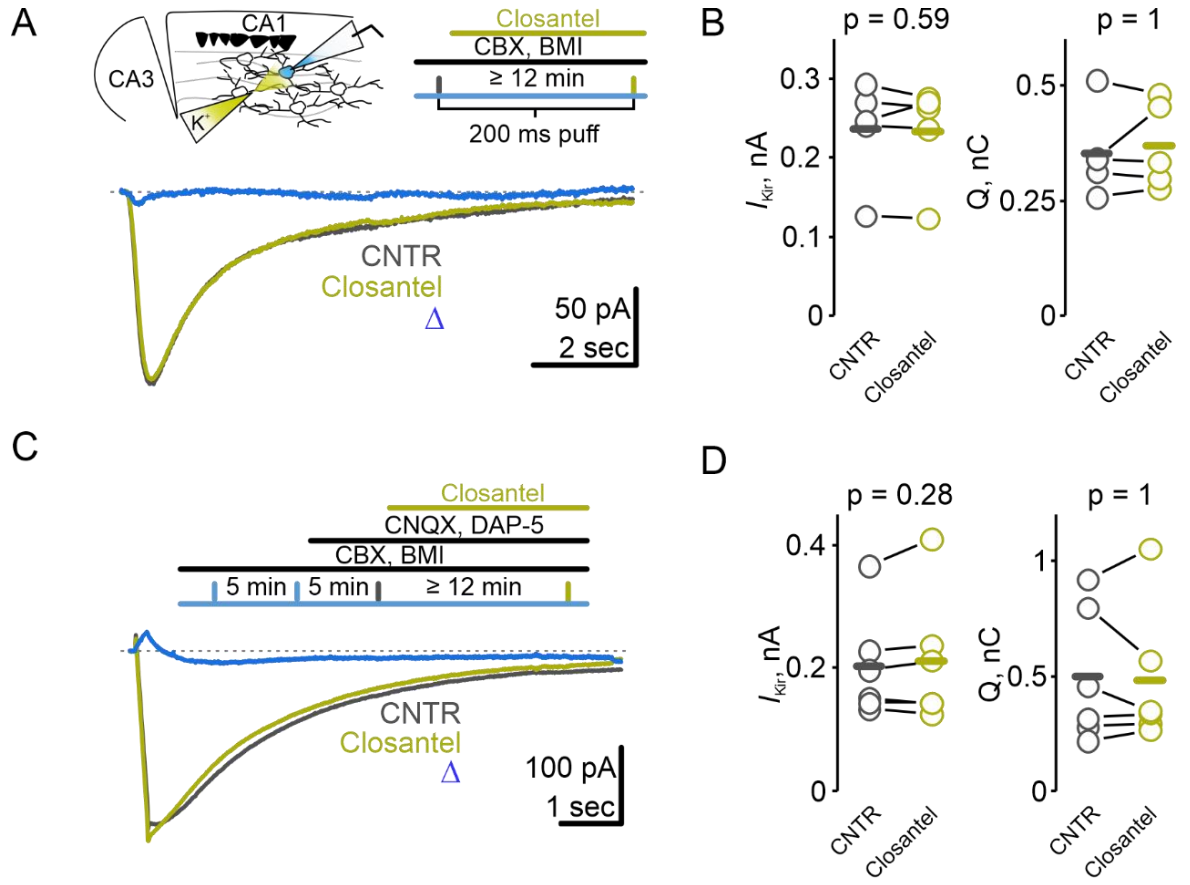

Figure 18. Closantel did not affect the K^+ uptake capacity of astrocytes when AMPA and NMDA receptors were blocked. **A** No off-target effect of closantel on the astrocytic membrane. Top left: scheme of the experiment; top right: timeline of the experiment; bottom: example traces under control conditions (*black*) and with closantel (*gold*) and the difference between the two (*blue*). **B** Closantel (10 μM) did not affect astrocytic peak I_{Kir} and Q in response to pressure ejection ACSF with increased K^+ (30 mM) onto an astrocyte isolated from the astrocytic syncytium by CBX ($I_{Kir\text{-}cntr}$ = 235 ± 29 pA, $I_{Kir\text{-}closantel}$ = 233 ±28 pA; n = 5; Q_{cntr} = 351 ± 42 pC, $Q_{closantel}$ = 368 ± 42 pC, n = 5, WSR). **C** Non-AMPA or NMDA-mediated $[K^+]_o$ elevation is insensitive to closantel. Top: timeline of the experiment; bottom: example traces of control (*black*) and with Closantel (*gold*) and the difference between the two (*blue*). **D** Residual astrocytic peak I_{Kir} and Q after blocking NMDA receptors (DAP-5, 25 μM) and AMPA receptors (CNQX, 20 μM), was not altered by closantel (10 μM) ($I_{Kir\text{-}cntr}$ = 204 ± 36 pA, $I_{Kir\text{-}closantel}$ = 212 ±43 pA; n = 6; Q_{cntr} = 497 ± 119 pC, $Q_{closantel}$ = 478 ± 123 pC, n = 6, WSR) with gap-junctions blocked by CBX.

Altogether, data presented so far indicate that KCC2 is an active contributor to K^+ ionostasis during moderate neuronal activity. Active KCC2 in reverse mode released peak and overall K^+ uptake load from astrocytes and putatively from other K^+ uptake mechanisms (e.g. Na^+/K^+-ATPase) when the tissue was under elevated but physiologically plausible excitatory stress. Experimental data showed up to 30% increase of peak I_{Kir} and Q when KCC2 was blocked. Enhancing KCC2 revealed up to 15% decrease in peak I_{Kir} and Q but only when astrocytic

gap-junctions were blocked. This detail suggests that a substantial portion of current detected by the patch electrode represents the lower band of the real range of astrocytic current and that the detected KCC2-mediated change somewhat underestimated real values. Despite this fact, KCC2 provides a considerable aid during abrupt and massive K^+ release upon AMPA and NMDA activation.

3.5 KCC2 reversal during weak synaptic activity, but not during single stimuli, is uncovered after impairing the astrocytic syncytium

The stimulation pattern used in previous experiments (20 pulses at 100 Hz) activates a large population of synapses therewith causing a rather strong K^+ release. Such events are possible, but not usual, during normal conditions, at least in brain slices. According to my hypothesis, KCC2 reverse mode only happens if $[K^+]_o$ reaches and passes beyond a certain reverse point in KCC2 driving force. That implies a direct dependence of KCC2 reverse probability on intensity and rate of synaptic activation. Therefore, I next asked if the KCC2 impact on peak I_{Kir} and Q persists during weaker stimulation, which is closer to common physiological activity. I lowered the number of pulses to 5 and the interpulse interval to 50 ms (20 Hz). This pattern does not usually induce LTP (Hashimotodani et al., 2017), but, since $GABA_A$ receptors were blocked, even such weak stimulation might induce LTP and affect astrocytic responses. To estimate the degree of possible potentiation I sampled peak I_{Kir} and Q responses at T_0 and 12 minutes later (at T_{12}). Additionally, I omitted preconditioning slices with two previously used trains of 20 pulses at 100 Hz – this removed unnecessary and inevitable modification of synaptic transmission associated with LTP (e.g. change in number of synapses, increase in receptors contents and expression, morphological changes of synapses etc.) that could cause ambiguity of results interpretation. As in previous experiments (Figure 9), I used parallel astrocytic patch clamp and fEPSP recordings to monitor possible changes in both astrocytic and neuronal activity (Figure 19).

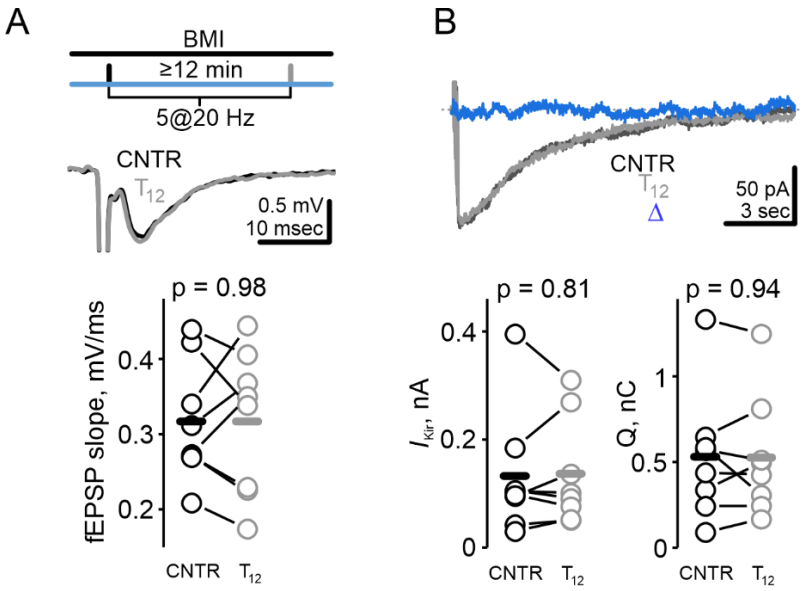

Figure 19. Weak stimulation (5 pulses at 20 Hz) did not induce long term field potential changes when $GABA_A$ receptors were blocked. **A** fEPSP averaged 3 min before (CNTR) and stimulation (T_{12}) remained similar (fEPSP $_{slopecntr}$ = 0.317 ± 0.028 mV/ms, fEPSP $_{slopeT12}$ = 0.317 ± 0.034 mV/ms; n = 8, pTT). Top: timeline of the experiment; middle: example fEPSP traces – control (*black*) and at T_{12} (*grey*); bottom: population data on fEPSP slopes. **B** Weak stimulation did not increase astrocytic peak I_{Kir} or Q ($I_{Kir\text{-}cntr}$ = 132 ± 41 pA, $I_{Kir\text{-}T12}$ = 136 ± 35 pA, n = 8; Q_{cntr} = 530 ± 132 pC, Q_{T12}= 526 ± 124 pC, n = 8, pTT). Top: example traces under control conditions (*black*), at T_{12} (*grey*) and the difference between the two (*blue*); bottom: population data on peak I_{Kir} and Q. Together with the data from (**A**) this allows to assess the effect of KCC2 block without preconditioning.

Neither fEPSP nor peak I_{Kir} and Q was amplified by the weak stimulation protocol. These results suggested that the used stimulation pattern did not potentiate CA3-CA1 synapses and that there was, indeed, no necessity in preconditioning the slices to mitigate LTP-associated modifications of synapses. Expectedly, the weak stimulation protocol elicited smaller $[K^+]_o$ elevation as astrocytic response was several-fold lower compared to moderate stimulation. Next, I blocked KCC2 with VU0463271 and analysed the outcome (Figure 20).

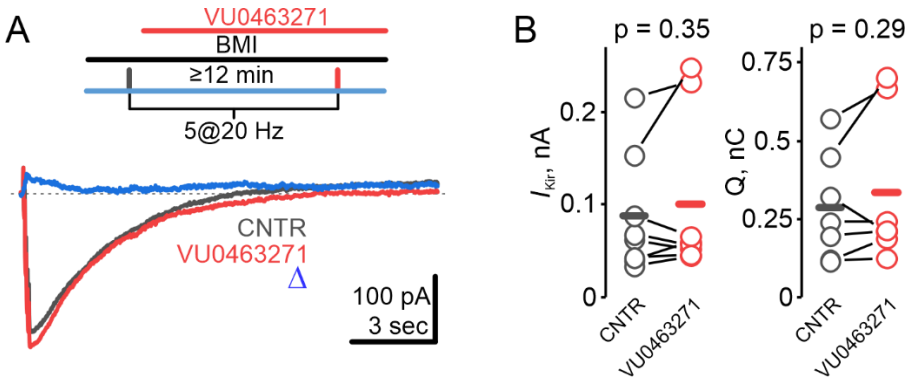

Figure 20. KCC2 block did not have any detectable effect on peak I_{Kir} and Q during the weak stimulation protocol. **A** Top: timeline of the experiment; bottom: example traces without (*black*) and with VU0463271 (*red*) and the difference between the two (*blue*). **B** VU0463271 (10

μM) application did not significantly change astrocytic peak I_{Kir} or Q ($I_{Kir\text{-}cntr}$ = 88 ± 23 pA, peak $I_{Kir\text{-}VU}$ = 101 ± 31 pA, n = 8; Q_{cntr} = 287 ± 65 pC, Q_{VU} = 336 ± 91 pC, n = 7, pTT).

Although there appeared to be a tendency of the astrocytic response towards increase (≈ 15%), statistics revealed no significant difference between control conditions and with VU0463271. This indicated that either a) weak stimulation failed to elevate $[K^+]_o$ large enough for KCC2 to reverse or b) that, due to large "leak" through astrocytic membrane, the signal was not strong enough to be registered. Because of this I implemented the same method of increasing astrocytic "sensitivity" with CBX. I ensured that exposure to CBX before control trace was recorded resulted in > 15 min as in experiments with moderate stimulation. CBX unmasked ≈ 34% increase in peak I_{Kir} and Q (Figure 21) which is comparable to change during moderate stimulation.

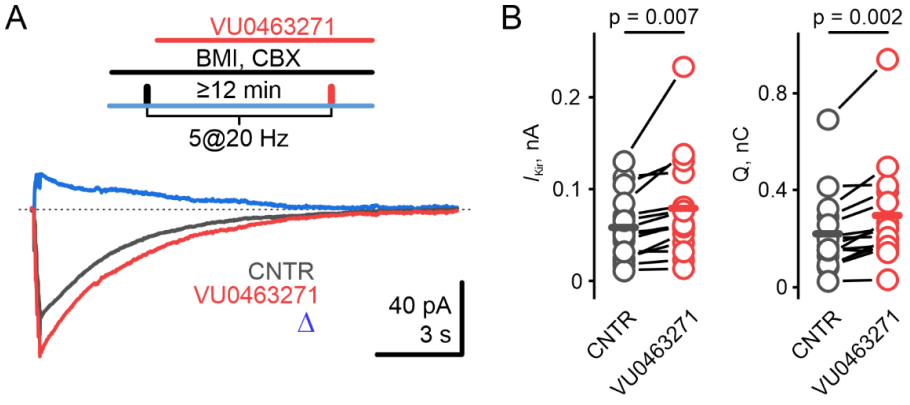

Figure 21. Disabling the astrocytic syncytium with CBX (100 μM) revealed the VU0463271-mediated (10 μM) increase of peak I_{Kir} and Q during weak stimulation. **A** Top: timeline of the experiment; bottom: example traces without (*black*) and with VU0463271 (*red*) and the difference between the two (*blue*). **B** Block of KCC2 during compromised astrocytic syncytium increased peak I_{Kir} and Q ($I_{Kir\text{-}ctrl}$ = 58 ± 9 pA, $I_{Kir\text{-}VU046327}$ = 78 ± 14 pA, n = 16, pTT; Q_{cntr} = 219 ± 43 pC, $Q_{VU0463271}$ = 297 ± 56 pC, n = 15; WSR). Adapted from (Byvaltcev et al., 2023). Adapted from (Byvaltcev et al., 2023).

The bath application of CBX might result in a range of neuronal and astrocytic effects that may not be solely attributed to the blocking of gap junctions (Verselis and Srinivas, 2013). Such effects – if present – might confound results and cause misinterpretation of the data when CBX was applied extracellularly (as in figures 17 and 21). Therefore, in some experiments from Figure 21 I applied CBX intracellularly to minimise its possible off-target effects (e.g., alteration of excitatory and inhibitory synaptic currents, intrinsic membrane properties, suppression of action potentials, Ca^{2+} channel block). I limited use of CBX only to the patched astrocyte by adding a lower concentration of CBX (25 μM) directly to the patch pipette and

monitored the efficiency of astrocytic isolation with Alexa Fluor 594 (25 µM) diffusion in real time (Figure 22A). Intracellular application of CBX revealed a rise in peak I_{Kir} and Q upon KCC2 block comparable to experiments when CBX was present in the ACSF (Figure 22B), rendering previously recorded peak I_{Kir} and Q increase independent from off-target effects of CBX.

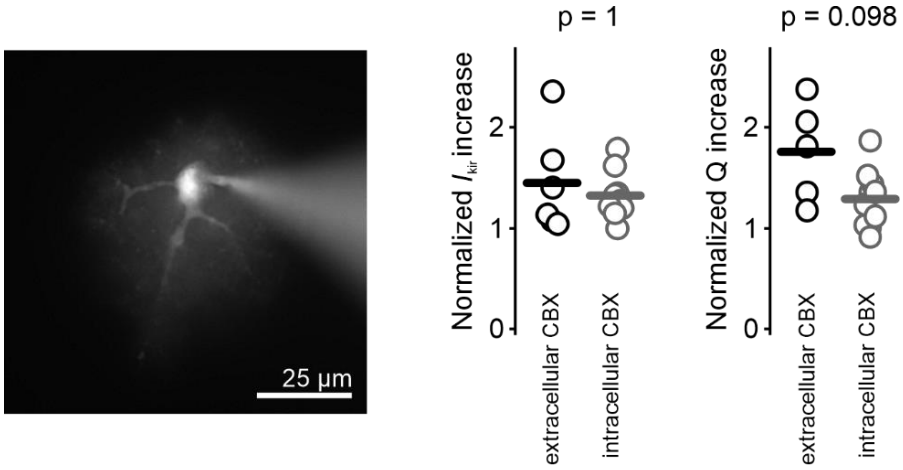

Figure 22. The effect of CBX restricted to the recorded astrocyte by intracellular application. Under that condition the increase in peak I_{Kir} and Q upon weak stimulation and KCC2 block with VU0463271 was comparable to the one revealed under extracellular CBX (normalized $I_{Kir\text{-}VU}$: extracellular CBX = 1.45 ± 0.21, n = 6, intracellular CBX = 1.32 ± 0.07, n = 10; normalized Q_{VU}: extracellular CBX = 1.76 ± 0.22, n = 5, intracellular CBX = 1.29 ± 0.09, n = 10, MWt). This renders putative slowly developing (neuronal) off-target effects of CBX unlikely. Left: The astrocyte under study was properly isolated as controlled with Alexa Fluor 594 (25 µM) that has been shown to monitor gap junction coupling (Anders et al., 2014) reliably and sensitively; right: population data on respective normalized peak I_{Kir} and Q increase.

Acquired data shows that both, moderate and weak stimulation, protocols caused KCC2-mediated decrease in peak I_{Kir} and Q, although, the effect of KCC2 during weak stimulation was harder to detect. I hypothesised that further weakening of stimulation and, consequently, lowering the intensity of neuronal postsynaptic activity would make KCC2 impact undetectable, at least with the methods I used. To investigate if this is the case, I implemented a stimulation protocol in which I applied only a single pulse but varied its intensity from 0.05 mA to 0.85 mA with 0.1 mA increments (Figure 23). I used intracellular application of CBX because experiments without it showed no significant change even with the weak stimulation protocol. Increasing stimulation intensity initially caused a steep rise in astrocytic response but eventually reached plateau and VU0463271 did not induce any change in peak I_{Kir}. These results suggest that even strong but single event stimulation was unable to elevate $[K^+]_o$ to required levels for KCC2 reverse point or for detection of such event.

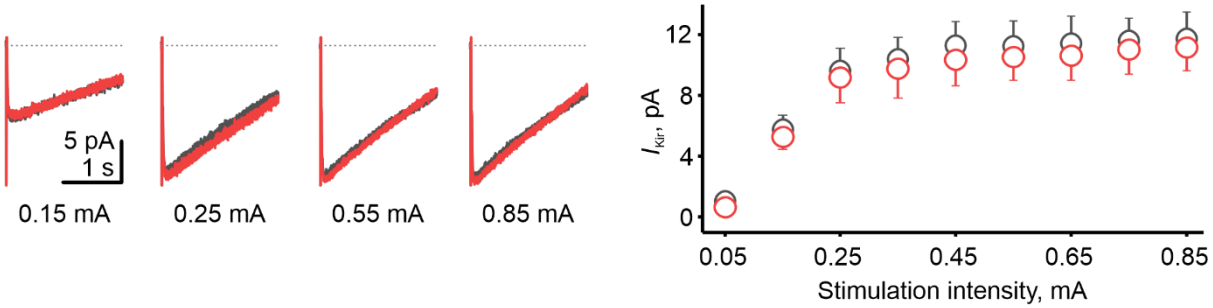

Figure 23. Single pulse stimulation did not change the peak I_{Kir} after KCC2 block with VU0463271 (gap-junctions were blocked by intracellular application of CBX). Left: example traces without (*black*) and with VU0463271 (*red*); right: population data on peak I_{Kir} plotted against stimulation intensity (n = 6, WSR).

Unfortunately, current K^+ registration methods lack the opportunity for detection of fast events with spatial resolution scale comparable to synaptic cleft to distinguish between 2 possible reasons of lack of astrocytic change during weak stimulation: a) low $[K^+]_o$ elevation and mere absence of KCC2 reverse mode, or b) low relative impact of KCC2 on astrocytic K^+ uptake current. Nevertheless, during abrupt and large synaptic activity-mediated K^+ release KCC2 transport activity in intake mode substantially reduces peak astrocytic K^+ uptake.

Taken together, experiments with weak and single pulse stimulation support my hypothesis that KCC2 reverse mode depends on repetitive neuronal postsynaptic activity and requires prolonged and significant K^+ release.

3.6 KCC2 modulation affects synaptic plasticity

In normal conditions all-over $[K^+]_o$ is kept at low levels as its elevation causes depolarisation of nearby membranes and augments excitability (Poolos et al., 1987). Such positive shift increases the glutamate release probability from the presynaptic bouton (Shih et al., 2013) and in general makes it easier for neurons to reach the action potential threshold. Consequently, impaired K^+ removal leads to augmented postsynaptic signalling and further K^+ release forming a positive feedback loop. I questioned whether such behaviour could be recorded in CA1 neurons when KCC2 is blocked, and the tissue is under greater K^+ accumulation stress. As peak I_{Kir} and K^+-sensitive electrodes showed, the highest $[K^+]_o$ elevation is observed immediately after stimulation and persists for 2 - 5 s thereafter. I looked for any changes in spontaneous excitatory post-synaptic currents (sEPSC) in the first seconds after moderate stimulation in CA1 pyramidal neurons. Usually, spontaneous presynaptic

glutamate release probability is estimated with miniature EPSC (mEPSC) with blocked action potentials by TTX. But in this case synaptic transmission is fully abolished as well as, consequently, any postsynaptic substantial $[K^+]_o$ elevations. VU0463271 showed no effect on baseline synaptic activity including frequency of sEPSC (Figure 13), meaning that any feasible change caused by KCC2 block is likely connected with increased $[K^+]_o$. As with astrocytic recordings during moderate stimulation I preconditioned the slices with 2 stimulations prior control trace recording to exclude LTP derived boost of sEPSC (Figure 24).

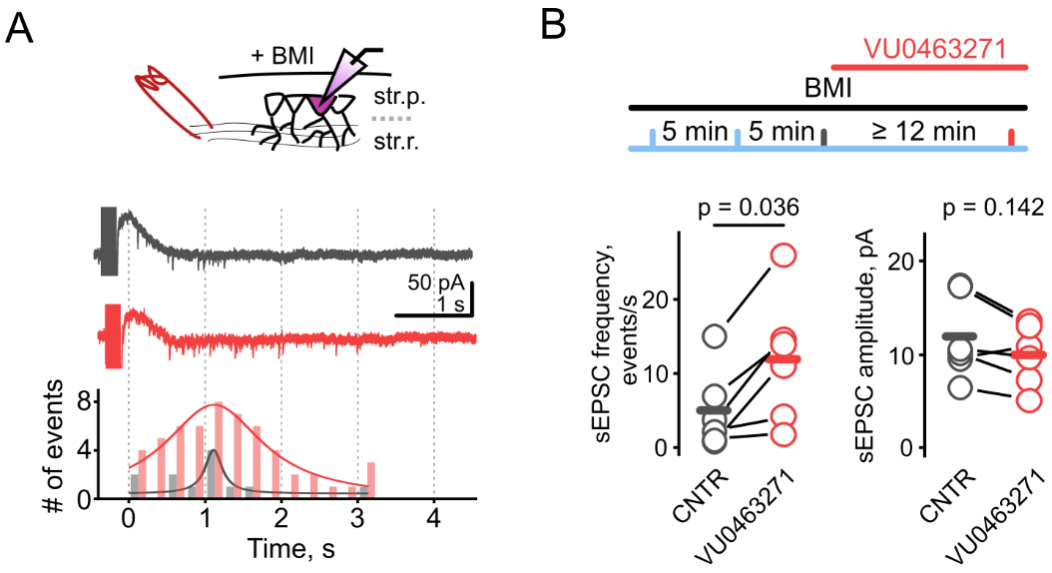

Figure 24. KCC2 block affected post-stimulation sEPSC frequency. **A** Top: experiment scheme; bottom: neuronal control (*black*) and with VU0463271 (*red*) example traces and binned # of events (bin size = 250 ms, Lorentz curve fitting). Note: most sEPSC frequency changes occurred within 2 – 3 s after stimulation. **B** KCC2 inhibition results in increased frequency but not amplitude of early (0 - 4 sec) post-stimulation sEPSC in CA1 pyramidal neurons (f_{ctrl} = 5.0 ± 2.2 events/s, f_{VU}= 12 ± 3.5 events/s, n = 6; $I_{EPSCctrl}$ = 11.9 ± 1.8 pA, I_{EPSCVU} = 9.9 ± 1.3 pA, n = 6, WSR). Top: timeline of the experiment; bottom: population data on peak I_{Kir} and Q. Adapted from (Byvaltcev et al., 2023).

Data revealed an increased frequency but an unaltered amplitude of sEPSC in the first seconds after stimulation when KCC2 was blocked. This suggests that presynaptic vesicular glutamate release was augmented while postsynaptic receptors properties remained without change ($\tau_{rise\text{-}cntr}$ = 3.2 ± 0.2 ms, $\tau_{rise\text{-}VU}$ = 3.5 ± 0.3 ms, n = 6, p = 0.4; $\tau_{decay\text{-}cntr}$ = 5.5 ± 0.8 ms, $\tau_{decay\text{-}VU}$ = 5.2 ± 0.7 ms, p = 0.29, n = 6; WSR). It is worth noting, that most of the sEPSC events took place in the first 2 seconds, which is roughly corresponding to peak currents recorded in astrocytes and by K^+-sensitive electrodes (Figure 10). I further assumed that if diminished KCC2 activity boosted glutamate release from presynaptic bouton, then the opposing effect from augmented

KCC2 transport activity should reduce sEPSC frequency. I implemented the same stimulation protocol substituting KCC2 blocker with closantel but also added CBX as it proved to be effective in unmasking the effect of closantel previously (Figure 25).

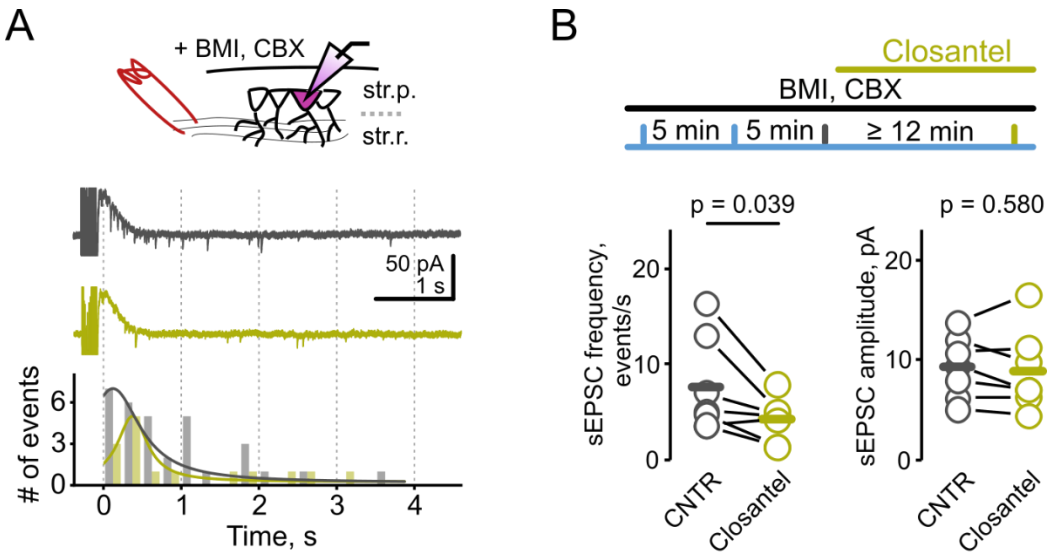

Figure 25. Facilitation of KCC2 during disrupted connexins decreased frequency of post-stimulation sEPSC. **A** Top: experiment scheme; bottom: neuronal control (*black*) and with closantel (*gold*) example traces and binned # of events (bin size = 250 ms, Lorentz curve fitting). Note: most sEPSC frequency changes occurred within 2 – 3 s after stimulation. **B** When gap-junctions were closed by CBX (100 μM), closantel reduced the frequency of post-stimulations sEPSC in CA1 pyramidal neurons leaving their amplitude unchanged (f_{ctrl} = 7.6 ± 1.9 events/s, $f_{closantel}$ = 4.1 ± 0.8 events/s, n = 7; $I_{EPSCctrl}$ = 9.2 ± 1.1 pA, $I_{EPSCclosantel}$ = 8.9 ± 1.5 pA, n = 7). Top: timeline of the experiment; bottom: population data on peak I_{Kir} and Q. Adapted from (Byvaltcev et al., 2023).

Acquired results supported the expected reduction of sEPSC frequency by closantel. As in the case with VU0463271, the amplitude of sEPSC remained unchanged as well as rise- and decay constant ($\tau_{rise\text{-}cntr}$ = 4.1 ± 0.4 ms, $\tau_{rise\text{-}closantel}$ = 3.5 ± 0.3 ms, n = 7, p = 0.17; $\tau_{decay\text{-}cntr}$ = 10.7 ± 1.8 ms, $\tau_{decay\text{-}closantel}$ = 9.8 ± 1.8 ms, p = 0.29, n = 7, pTT). KCC2 enhancement augmented $[K^+]_o$ uptake and by that reduced presynaptic glutamate release compared to control. It is worth pointing out, that in both previous cases neuronal recordings were made in voltage clamp mode thus reducing probability of NMDA receptors to release Mg^{2+}. This renders the registered KCC2 effect underestimated as NMDA receptors mediate majority of $[K^+]_o$ increase during glutamatergic transmission (Shih et al., 2013).

Recorded KCC2-mediated alteration of postsynaptic sEPSC might influence the efficiency of activity sensitive plasticity such as LTP. An earlier study demonstrated that diminished KCC2

induces stronger LTP while enhancing KCC2 showed no effect (Ferando et al., 2016). This was connected to GABAergic transmission and involved changing $[Cl^-]_i$. Since in my experimental protocols the inhibition was blocked and there was no significant $[Cl^-]_i$ alteration, I questioned how blocking or enhancing KCC2 would impact long term synaptic plasticity with blocked $GABA_A$ receptors. Because activation of NMDA receptors is crucial for induction of plasticity, neurons should be free to fluctuate their V_m and generate action potentials. Additionally, recording fEPSP is a more reliable method as it provides averaged resulting signal of induced LTP. Accordingly, instead of neuronal patch clamp recordings I conducted classical LTP induction experiments gauging fEPSP slopes. In this set of experiments, I did not use any preconditioning stimulations to get unbiased potentiating capacity. For LTP induction I used moderate stimulation implemented earlier (20 pulses at 100 Hz) (Figure 26).

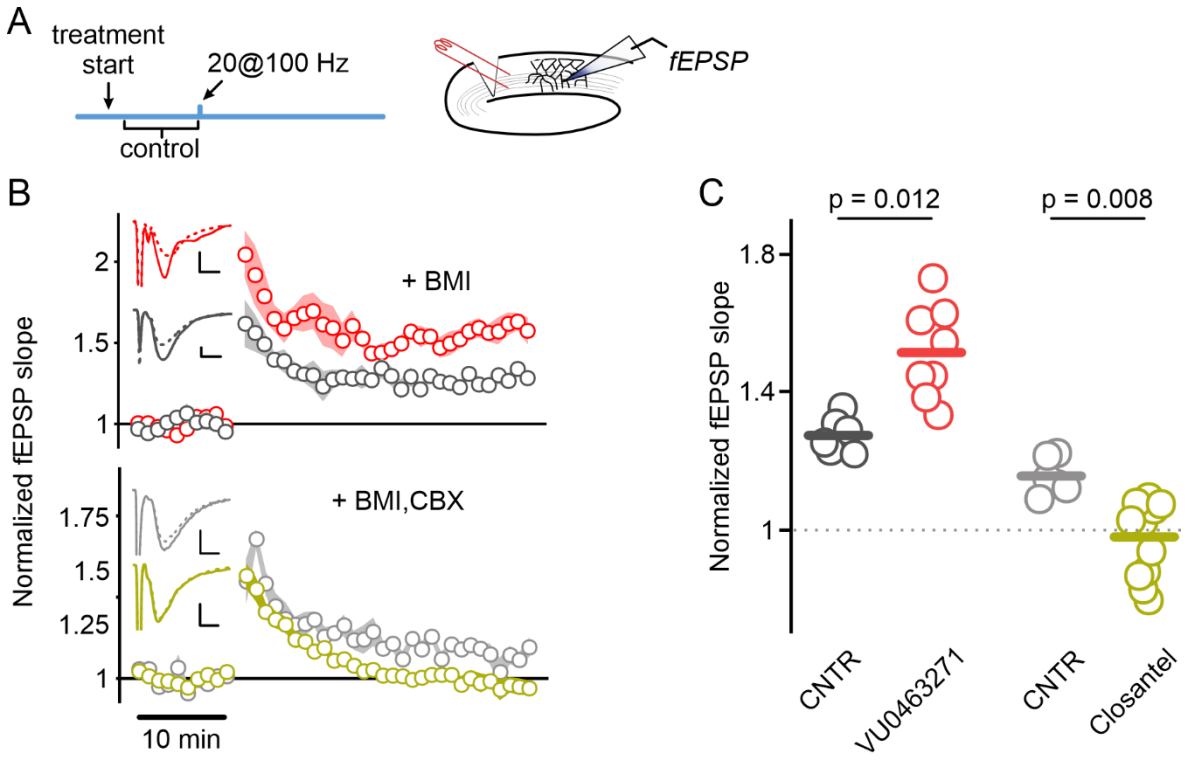

Figure 26. Synaptic potentiation modulated by KCC2 efficiency. **A** Left: timeline of the experiment; right: scheme of the experiment. **B** KCC2 block augmented LTP (upper panel, VU0463271, *red*, LTP_{cntr} = 1.27 ± 0.03, n = 6; LTP_{VU} = 1.51 ± 0.06, n = 8, MWT), whereas enhancing KCC2 attenuated LTP (lower panel, closantel, *gold*, $LTP_{cntr\text{-}CBX}$ = 1.16 ± 0.03, n = 6; $LTP_{closantel\text{-}CBX}$ = 0.98 ± 0.04, n = 11, MWT) compared to the respective control (*black* and *gray*). Insets: averaged fEPSP traces before (dotted) and after (solid) LTP induction. Scale bars: 5 ms, 0.25 mV. **C** Population data of fEPSC slopes normalized and averaged (20 – 30 min after LTP induction). Adapted from (Byvaltcev et al., 2023).

Interestingly, as in the study by Ferando et.al., KCC2 block augmented LTP suggesting that together with $[Cl^-]_i$, at least partially, this boosted potentiation effect can be attributed to $[K^+]_o$ as well. Addition of CBX alone slightly reduced LTP (Chepkova et al., 2008), while closantel almost completely abolished LTP induction. Of note, during the first minutes after stimulation, fEPSP were similarly potentiated both with and without closantel which seems to prevent LTP preservation in the long run.

In summary, the blockade of KCC2 resulted in increased presynaptic glutamate release and heightened excitatory transmission, while enhancing KCC2 activity reduced glutamate release, suggesting KCC2's pivotal role in regulating excitation balance. Acquired data also reveals KCC2 participation in fundamental physiologically important mechanisms of excitation balance and information processing and storage. KCC2 attenuates excess K^+ release during transient and intense excitatory signalling damping excitotoxic peaks of $[K^+]_o$.

4. Discussion

Ionic signalling mechanisms exert a broad influence on local cell types and structures, including neuronal membrane components like dendrites, spines, and axons. These mechanisms play a crucial role in modulating excitability, synaptic plasticity, and, in extreme cases, neuronal survival. However, our understanding of ion-mediated modulation of synaptic transmission remains limited due to technical challenges, including spatial and temporal resolution limitations, a lack of appropriate recording methods, and the inherent stochastic nature of processes in micro- to nanoscale environments.

4.1 KCC2 reverse mode clears $[K^+]_o$

Here, I have addressed the role of KCC2 in regulation of $[K^+]_o$ in the perisynaptic area of excitatory CA3-CA1 synapses in the murine hippocampus. To overcome difficulties of recording fast activity dependent changes of $[K^+]_o$ in synaptic microenvironment, I have implemented astrocytic patch-clamp recordings accompanied by recordings with slower K^+-sensitive electrodes. Each astrocyte occupies a certain volume of neuropil called domain, within which all synapses are “serviced” by this single astrocyte. The majority of astrocytic PAPs is located very close to synaptic clefts and can even enwrap the whole synapse. Additionally, PAPs are enriched in K_{ir} channels, that are highly sensitive to $[K^+]_o$ changes. These aspects allowed to record astrocytic currents elicited by synaptic activity dependent changes of $[K^+]_o$ with a higher sensitivity and a much smaller delay than with K^+-sensitive electrodes (Figure 10). Using this approach, I showed that KCC2 attenuates astrocytic K^+ uptake during abrupt and moderate glutamatergic activity. Also, the modification of KCC2 function impacted presynaptic glutamate release and LTP strength. Altogether, these findings support recent studies that KCC2 is more than just a passive K^+ and Cl^- extruder even under physiological conditions and it has a complex reciprocal connection with neurotransmission.

In detail, I found that KCC2 substantially helps clearing perisynaptic K^+ during synaptic activity by temporarily changing K^+ and Cl^- transport direction to inward. Such ion uptake mode mitigates excess presynaptic depolarisation and counteracts the excitation positive feedback loop, in which glutamate release causes K^+ efflux causing more glutamate release. Furthermore, as KCC2 is localised near excitatory synapses (Chamma et al., 2013) such ionic uptake also prevents K^+ spillover which also limits K^+-derived depolarisation – another hint that KCC2 assists astrocytes in signal isolation. In this way, KCC2 limits excess excitation not only by maintaining GABA action hyperpolarising (keeping $[Cl^-]_i$ at low values) but also by curtailing abrupt $[K^+]_o$ elevations. In addition, as attenuating of high $[K^+]_o$ is crucial for effective

astrocyte-mediated glutamate uptake mechanism (Tyurikova et al., 2022), facilitated presynaptic glutamate release upon reduced KCC2 activity might contribute to the proposed feedforward K^+ accumulation (Grafstein, 1956).

In mature neurons compromised KCC2 disrupts proper inhibition (Rivera et al., 1999) and KCC2 decline during senescence causes facilitation of LTP (Ferando et al., 2016). In conditions of hindered Cl^- extrusion GABAergic inhibition either loses efficiency or even reverses polarity (to outwardly directed Cl^- flux) and contributes to the increase of Ca^{2+} influx during glutamate-dependent depolarisation (Ferando et al., 2016). Moreover, Ferando et al. suggested that the depolarising action of $GABA_A$ receptors might elicit $[Ca^{2+}]_i$ increase in dendrites and synapses that initially were not activated, therewith spreading potentiation beyond the targeted synapse cluster. Therefore, functional and unaltered KCC2 contributes to synaptic specificity and prevents activation of non-targeted inputs by maintaining adequate inhibition (Ferando et al., 2016). In a way, this resembles astrocytic PAPs and their role in restraining glutamate spillover from active excitatory synapses to silent ones. This can be attributed as signal isolation function that keeps synaptic segregation and action-target specificity intact especially during multiple synapse activation and LTP. And on contrary, diminished KCC2 might contribute to spread of potentiation to neighbouring synapses (Harvey and Svoboda, 2007).

Note that to this point KCC2 was not considered as a significant, if any at all, contributor to $[K^+]_o$ regulation under physiological conditions – the majority of handling excess K^+ was justly attributed to Na^+/K^+-ATPase, astrocytes and passive diffusion. My proposed temporary transport reverse mode of KCC2 adds to a variety of ways to minimise excitotoxic effects of high $[K^+]_o$. As suggested above, for KCC2 to start contributing to clearance of extracellular K^+ load, it probably requires stronger activity-dependent K^+ release than during single synaptic activation (e.g. repetitive multisynaptic excitatory signalling). Although, my single pulse protocol did not show any change after KCC2 block, these measurements should be verified with other, potentially more precise methods (e.g. optical K^+ sensors, modelling) as reverse of KCC2 might be achievable even with low amplitude $[K^+]_o$ rise given low $[Cl^-]_i$ (DeFazio et al., 2000; Payne, 1997). Nevertheless, such events occur in both, physiological (e.g. brain rhythms, LTP) and pathological conditions (e.g. seizures).

There are several potential physiologically relevant consequences of the reverse mode in KCC2 flux. Firstly, by providing “additional” yet temporary sink for K^+ in spines, KCC2 mitigates extremes and flattens the kinetics of sudden rises of $[K^+]_o$ (Figure 27). Notably, while smoothening $[K^+]_o$ peaks, KCC2 might prolong the exposure of local neuropil to K^+ rise when it restores outward transport. So, overall $[K^+]_o$ load remains the same but KCC2 allows for

more time to counteract the stress. Secondly, it is not clear whether K^+ loaded to the spine during high levels of $[K^+]_o$ is fully re-ejected back to ECS by KCC2 that has returned to extrusion. Part of the "(re)imported" K^+ could replenish losses in $[K^+]_i$ due to AMPA and NMDA opening. Thirdly, flattening excess K^+ peaks and reloading spine with K^+ by KCC2 releases stress from primary buffering mechanisms (particularly from Na^+/K^+-ATPase both neuronal and astrocytic) and by this reducing energy required to restore ionic concentrations.

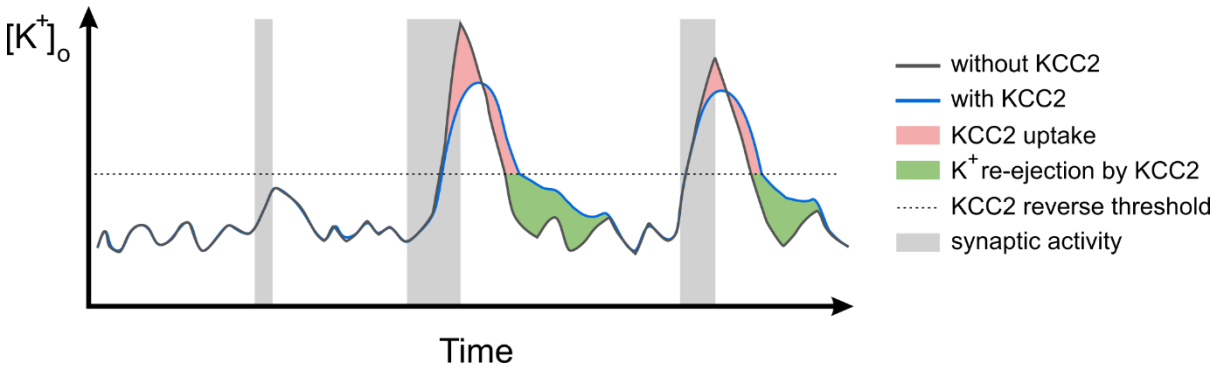

Figure 27. Scheme of possible KCC2 reverse mode effect on $[K^+]_o$ during excitatory activity. Note: here KCC2 threshold is constant and serves as a conceptual representation rather than an exact depiction of the process – in real conditions this threshold level depends on both $[K^+]_o$ and $[Cl^-]_i$.

Temporal K^+ buffering by reversed KCC2 might aid the restoration of NMDA receptor activity and pain threshold in neuropathic pain conditions after KCC2 overexpression (Li et al., 2016). Also, when other $[K^+]_o$ clearance mechanisms are overloaded (e.g. disrupted astrocytic syncytium (Nakase and Naus, 2004)) K^+ uptake by KCC2 possibly can extend resilience of the network against synchronized "epileptic" activity. However, if GABAergic signaling is prevailing and there is little $[K^+]_o$ stress, KCC2 rather facilitates ictal activity by actually elevating $[K^+]_o$ during restoring $[Cl^-]_i$ (Viitanen et al., 2010). Still, temporal engagement of KCC2 into $[K^+]_o$ clearance adds another perspective to already existing data on KCC2 participation in seizures, neuropathic pain and spreading depression (Hyde et al., 2011; Kahle et al., 2008; Magloire et al., 2019; Mapplebeck et al., 2019; Moore et al., 2017).

Recent neuroinflammation-focused research revealed dependance of KCC2-mediated transport from lipopolysaccharide induced inflammatory mechanisms (Kurki et al., 2023). In parallel with downregulated Cl^- extrusion via KCC2 Kurki et al. found potentiated NKCC1 activity that together caused Cl^- loading of neurons and, consequently, disrupted inhibition. Interestingly, our previous research (Janach et al., 2020) showed that the proinflammatory interferon-γ alone rather increases inhibition. A reciprocal regulation of KCC2 and NKCC1 is

also a common condition found in spinal cord after injury (Talifu et al., 2022). This suggests that KCC2 together with NKCC1 (sometimes controlled by the same regulatory cascades) might serve as one of the intermediatory proteins in excitation and inhibition crosstalk.

4.2 Modelling KCC2 reverse mode

In collaboration with Mahraz Behbood, Jan-Hendrik Schleimer, Susanne Schreiber and Ulf Strauss we devised a model of synaptic cleft to clarify putative KCC2 reverse and get equation-based proof of principle (Byvaltcev et al., 2023). This approach allowed us to overcome some of the limitations of direct experimental observation of KCC2 ions flux. The model explored the exchange of K^+ and Cl^- among the effective spine, perisynaptic extracellular space (pECS), and astrocyte compartments. By simplifying the model, we aimed to focus on the essential biophysical factors governing KCC2 transport and its temporal dynamics. In brief, the model showed that following transient increase of $[K^+]_o$, the equilibrium potential shifted, favoring a temporary reverse mode of KCC2 which resulted in substantial K^+ uptake (along with Cl^-) into the effective spine compartment. The subsequent drop in $[K^+]_o$ and influx of Cl^- electrochemically triggered the direct mode of KCC2, gradually releasing K^+ from the spine compartment to the pECS that was absorbed by the Na^+/K^+-ATPase and K_{ir} channels. This pattern of KCC2 transport was in line with the temporal nature of $[K^+]_o$-dependent reverse proposed above. Also, the model made the differences to other K^+ clearance mechanisms depending on $[K^+]_o$ apparent — while K_{ir} channels and Na^+/K^+-ATPase contributed similarly with and without KCC2 under weak stimulation, K_{ir} channels' contribution became pronounced with moderate stimulation, especially in the absence of KCC2. This aspect supported the putative energy conservation effect of KCC2 reverse and might explain the clustering of transport active KCC2 near excitatory synapses.

We also aimed to investigate the spread of $[K^+]_o$ in a more spatially detailed manner and asked how KCC2 might affect $[K^+]_o$ distribution between synapses. Synaptic connections between CA3 and CA1 are typically about 0.5 µm apart on average, which poses challenges in studying synaptic spillover caused by varying activity between these neighbouring regions due to the lack of precise targeting in experiments. We divided pECS and spine compartments into active and inactive sections allowing for the diffusion of K^+. The activity of KCC2 determined the increase of $[K^+]_o$ in both extracellular compartments. While the diffusion time constant influenced the increase in $[K^+]_o$ in neighbouring compartments, the impact of KCC2 remained consistent across various timescales of diffusion. This result points out several aspects (and putatively future research questions): a) in addition to Cl^- based mechanism of synaptic isolation (Ferando et al., 2016), KCC2 might contribute to signal specificity via restraining K^+

spillover, and, accordingly, b) diminished KCC2 might increase synaptic synchronisation and reduce network resilience to overexcitation. Although, it is puzzling how are these potential "stabilising" properties connected to KCC2 mediation of excitotoxicity derived blebbing (Weilinger et al., 2022).

Altogether, the mathematical model supported my experimental data showing that KCC2 in reverse mode temporarily regulates $[K^+]_o$ during abrupt increases, distributing the workload of homeostatic mechanisms (K_{ir} channels and Na^+/K^+-ATPase) over time. Also, the model provided hints in KCC2-mediated synaptic isolation as blocked KCC2 influenced synaptic K^+ spillover.

4.3 Limitations and reservations

Although brain slices are widely used in brain research, this method might underestimate the true scale of KCC2 impact in intact *in vivo* brain conditions. Even with several neuroprotection measures slicing does mechanical damage which varies from slice to slice even within one preparation procedure. It is hard to validate neuropil recovery degree and how close it represents undamaged brain neuropil (Kirov et al., 1999). Another difficulty in determining KCC2-mediated impact is connected to the damage-associated $[Cl^-]_i$ accumulation in neurons close to the slice surface (Dzhala et al., 2012). High $[Cl^-]_i$ makes KCC2 reverse more challenging by shifting reversal threshold towards higher values of $[K^+]_o$, i.e. requires higher excitatory input. I addressed this issue by aiming for more deeply located astrocytes in patch-clamp experiments, however, due to highly arborised morphology, astrocytes might still be in contact with spines and dendrites of superficial "damaged" neurons.

Recording astrocytic current is well-suited for capturing localized perisynaptic $[K^+]_o$ fluctuations, as astrocytic PAPs are rich in K_{ir} channels and create separation from the ECS. However, these recordings may underestimate the role of KCC2 in perisynaptic $[K^+]_o$ uptake, as astrocytic K_{ir} channels represent only one of several K^+ uptake mechanisms. In addition, astrocytes might not be ideal for detection of entire effects due to low membrane resistance and losses of current through connexins (up to 30%) (Wallraff et al., 2006). Although blocking gap-junctions allowed to facilitate astrocytic "sensitivity" to some extent (Figures 17, 21), unique and complex geometry and spatial positioning of each astrocyte introduce great variability to such enhancement. In the experiments I conducted, the effect of KCC2 might be further attenuated by a decrease in membrane stability of KCC2 due to NMDA activation (Lee et al., 2011; Weilinger et al., 2022). In this way, increased membrane drift might disrupt KCC2 "accumulation" in the perisynaptic membrane. Although KCC2 membrane pool was shown to be diminished after $GABA_B$ activation (Wright et al., 2017), in the experimental set up I used

$GABA_B$ block showed no effect on peak I_{Kir} and Q. Nevertheless, regardless of the actual absolute effect size, results show that KCC2 transport directly modulates $[K^+]_o$ and glutamatergic neurotransmission. This suggests that any alteration of the KCC2 has a dual impact, influencing not only the efficiency of $GABA_A$-mediated inhibition but also exerting changes in the response to excitatory signals.

Perisynaptic $[K^+]_o$ and, consequently, synaptic transmission is dynamically regulated by KCC2, which, in turn, is modified by various posttranslational mechanisms (Medina et al., 2014). Notably, changes in neuronal activity can either increase or decrease KCC2 expression or activity, depending on various intracellular signalling pathways. Furthermore, KCC2 engages in interactions with a diverse range of proteins. While some of these proteins regulate KCC2 expression (Ivakine et al., 2013; Mahadevan and Woodin, 2016; Wright et al., 2017), others are reciprocally regulated by KCC2 (Chevy et al., 2015; Llano et al., 2015). One of such interactions augmented postsynaptic excitability through ionotropic TASK-3 channels (Goutierre et al., 2019). Although this effect was associated with KCC2 expression and not with ion translocation function, as application of VU0463271 failed to elicit similar changes and, thus, cannot directly explain our results. However, these two processes might simultaneously contribute to hyperexcitability when KCC2 is chronically diminished.

The absence of KCC2 recruitment upon the extracellular pressure ejection of elevated K^+, together with the rapid and seemingly more responsive detection of $[K^+]_o$ changes by astrocytes implies perisynaptic space to be rather distinct compartment of ECS. This phenomenon becomes more apparent when astrocytic recordings are compared with the relatively slow responses observed through ion-sensitive electrodes following synaptic stimulation — due to spatial and methodological limitations K^+-sensitive electrodes provide rather general and averaged ECS data than a perisynaptic readout. A parallel can be drawn with similar compartmentalization reported in the context of glutamate dynamics — previous research has indicated analogous partition for synaptic- and extrasynaptic glutamate levels and action (Wu et al., 2012), confirming the idea that distinct ECS compartments play a crucial, yet slightly varying, role in regulating neurotransmitter and ion homeostasis within the synaptic environment. Such ECS partition might resist and/or attenuate artificial $[K^+]_o$ elevation and accumulation near KCC2 in/at synapses preventing its reverse. The assumption of the perisynaptic space as a segregated ECS compartment gains further support from earlier investigations that highlighted source-dependent variations in the effects of elevated $[K^+]_o$, such as those observed under superfusion conditions *vs.* synaptic stimulation (Poolos et al., 1987).

4.4 Potential for further research

Yet both modes of KCC2 transport (influx and efflux) are shown to be closely connected with excitation and inhibition, exact and detailed mechanism of attenuating excitability by KCC2 remains unknown. Here, I have confirmed that KCC2 in ion uptake mode temporarily acts to dampen transient excitation inputs by buffering excess perisynaptic $[K^+]_o$ elevations. Together with the baseline activity of Cl^- extrusion in dendrites during a relatively silent excitatory synaptic state these two "states" of KCC2 might create a temporal, activity-dependent, and spatial segregation of network control. The described influx, which occurs in response to synaptic excitation, is temporal and appears to be coupled to the local microenvironment of excitatory synapses, particularly spines. This localised activity assists other $[K^+]_o$ buffering mechanisms in preventing the accumulation of extracellular potassium, maintain ionic homeostasis in the immediate vicinity of excitatory synapses and helps preventing potential excitotoxicity and hyperexcitability, thereby maintaining the optimal extracellular environment for sustained neuronal function. Conversely, the persistent efflux mediated by KCC2 is long-term, takes place at dendritic shafts and is sustained by elevations in $[Cl^-]_i$ resulting from synaptic inhibition. This efflux mechanism ensures low $[Cl^-]_i$ that is vital for the efficient inhibition (preservation of hyperpolarization mediated by $GABA_A$ receptors), thereby enhancing the overall inhibitory control within the neuronal network.

Speculatively, one could consider that the segregation of KCC2 effects in time and space and cooperative nature of these two effects allow for a sophisticated adaptive advantage to the neuronal network. In this way, the short bursts of influx near excitatory synapses could serve as a rapid response mechanism to prevent excessive excitation locally. Meanwhile, the persistent efflux at dendritic shafts might contribute to the long-term stability of inhibitory processes. The delicate balance maintained by KCC2 could be crucial for counteracting excess excitation and ensuring the fine-tuning of neuronal activity. However, when the function of KCC2 is compromised, as seen in various pathological conditions, it is plausible that both effects may degrade simultaneously. This degradation could result in a cascade of destabilising events, including impaired $[K^+]_o$ clearance, a loss of the long-term maintenance of low $[Cl^-]_i$ and inefficiency of inhibitory mechanisms, potentially contributing to neuronal hyperexcitability. Therefore, the KCC2-mediated fine balance putatively is a critical factor in preventing aberrant neuronal activity and excitotoxicity.

It is puzzling if these two "states" of KCC2 activity might take place simultaneously due to spatial separation and how they might be influencing each other. Such interaction would likely be mediated by interplay of $[Cl^-]_i$ and $[K^+]_o$ both in spine and dendritic shaft. Yet another level of complexity is added with known relation of excitation and inhibition with $[K^+]_o$ and $[Cl^-]_i$ respectively. Such multivariable processes require further investigations to unveil the precise

mechanisms underlying KCC2 bidirectional ionic transport and its signal processing modulation in neuronal networks.

In summary, this investigation has identified a temporary reverse mode of spine KCC2 that facilitates the clearance of elevated perisynaptic K^+ levels at excitatory synapses. This perspective strengthens the understanding of KCC2 as a pivotal player in modulating the balance between excitation and inhibition, not only during maturation but also in the adult brain. This influence extends to fundamental processes such as presynaptic glutamate release, LTP and the regulation of spillover events.

References

Afzalov, R., Pryazhnikov, E., Shih, P.-Y., Kondratskaya, E., Zobova, S., Leino, S., Salminen, O., Khiroug, L., Semyanov, A., 2013. Low micromolar Ba2+ potentiates glutamate transporter current in hippocampal astrocytes. Front. Cell. Neurosci. 7. https://doi.org/10.3389/fncel.2013.00135

Alagem, N., Dvir, M., Reuveny, E., 2001. Mechanism of Ba^{2+} block of a mouse inwardly rectifying K^{+} channel: differential contribution by two discrete residues. J. Physiol. 534, 381–393. https://doi.org/10.1111/j.1469-7793.2001.00381.x

Alvarez-Leefmans, F.J., 2012. Intracellular Chloride Regulation, in: Cell Physiology Source Book. Elsevier, pp. 221–259. https://doi.org/10.1016/B978-0-12-387738-3.00015-9

Anders, S., Minge, D., Griemsmann, S., Herde, M.K., Steinhäuser, C., Henneberger, C., 2014. Spatial properties of astrocyte gap junction coupling in the rat hippocampus. Philos. Trans. R. Soc. B Biol. Sci. 369, 20130600. https://doi.org/10.1098/rstb.2013.0600

Awad, P.N., Amegandjin, C.A., Szczurkowska, J., Carriço, J.N., Fernandes Do Nascimento, A.S., Baho, E., Chattopadhyaya, B., Cancedda, L., Carmant, L., Di Cristo, G., 2018. KCC2 Regulates Dendritic Spine Formation in a Brain-Region Specific and BDNF Dependent Manner. Cereb. Cortex 28, 4049–4062. https://doi.org/10.1093/cercor/bhy198

Báldi, R., Varga, C., Tamás, G., 2010. Differential distribution of KCC2 along the axo-somato-dendritic axis of hippocampal principal cells: KCC2 distribution along hippocampal principal cells. Eur. J. Neurosci. 32, 1319–1325. https://doi.org/10.1111/j.1460-9568.2010.07361.x

Bernardinelli, Y., Muller, D., Nikonenko, I., 2014a. Astrocyte-Synapse Structural Plasticity. Neural Plast. 2014, 1–13. https://doi.org/10.1155/2014/232105

Bernardinelli, Y., Randall, J., Janett, E., Nikonenko, I., König, S., Jones, E.V., Flores, C.E., Murai, K.K., Bochet, C.G., Holtmaat, A., Muller, D., 2014b. Activity-Dependent Structural Plasticity of Perisynaptic Astrocytic Domains Promotes Excitatory Synapse Stability. Curr. Biol. 24, 1679–1688. https://doi.org/10.1016/j.cub.2014.06.025

Blaesse, P., Guillemin, I., Schindler, J., Schweizer, M., Delpire, E., Khiroug, L., Friauf, E., Nothwang, H.G., 2006. Oligomerization of KCC2 Correlates with Development of Inhibitory Neurotransmission. J. Neurosci. 26, 10407–10419. https://doi.org/10.1523/JNEUROSCI.3257-06.2006

Burgstaller, S., Wagner, T.R., Bischof, H., Bueckle, S., Padamsey, A., Frecot, D., Kaiser, P.D., Skrabak, D., Malli, R., Lukowski, R., Rothbauer, U., 2022. Monitoring

extracellular ion and metabolite dynamics with recombinant nanobody-fused biosensors. iScience 25, 104907. https://doi.org/10.1016/j.isci.2022.104907

Bushong, E.A., Martone, M.E., Jones, Y.Z., Ellisman, M.H., 2002. Protoplasmic Astrocytes in CA1 Stratum Radiatum Occupy Separate Anatomical Domains. J. Neurosci. 22, 183–192. https://doi.org/10.1523/JNEUROSCI.22-01-00183.2002

Byvaltcev, E., Behbood, M., Schleimer, J.-H., Gensch, T., Semyanov, A., Schreiber, S., Strauss, U., 2023. KCC2 reverse mode helps to clear postsynaptically released potassium at glutamatergic synapses. Cell Rep. 42, 112934. https://doi.org/10.1016/j.celrep.2023.112934

Cardarelli, R.A., Jones, K., Pisella, L.I., Wobst, H.J., McWilliams, L.J., Sharpe, P.M., Burnham, M.P., Baker, D.J., Chudotvorova, I., Guyot, J., Silayeva, L., Morrow, D.H., Dekker, N., Zicha, S., Davies, P.A., Holenz, J., Duggan, M.E., Dunlop, J., Mather, R.J., Wang, Q., Medina, I., Brandon, N.J., Deeb, T.Z., Moss, S.J., 2017. The small molecule CLP257 does not modify activity of the K+–Cl− co-transporter KCC2 but does potentiate GABAA receptor activity. Nat. Med. 23, 1394–1396. https://doi.org/10.1038/nm.4442

Chamma, I., Chevy, Q., Poncer, J.C., Lévi, S., 2012. Role of the neuronal K-Cl co-transporter KCC2 in inhibitory and excitatory neurotransmission. Front. Cell. Neurosci. 6. https://doi.org/10.3389/fncel.2012.00005

Chamma, I., Heubl, M., Chevy, Q., Renner, M., Moutkine, I., Eugène, E., Poncer, J.C., Lévi, S., 2013. Activity-Dependent Regulation of the K/Cl Transporter KCC2 Membrane Diffusion, Clustering, and Function in Hippocampal Neurons. J. Neurosci. 33, 15488–15503. https://doi.org/10.1523/JNEUROSCI.5889-12.2013

Chepkova, A.N., Sergeeva, O.A., Haas, H.L., 2008. Carbenoxolone impairs LTP and blocks NMDA receptors in murine hippocampus. Neuropharmacology 55, 139–147. https://doi.org/10.1016/j.neuropharm.2008.05.001

Chevy, Q., Heubl, M., Goutierre, M., Backer, S., Moutkine, I., Eugène, E., Bloch-Gallego, E., Lévi, S., Poncer, J.C., 2015. KCC2 Gates Activity-Driven AMPA Receptor Traffic through Cofilin Phosphorylation. J. Neurosci. 35, 15772–15786. https://doi.org/10.1523/JNEUROSCI.1735-15.2015

Côme, E., Marques, X., Poncer, J.C., Lévi, S., 2020. KCC2 membrane diffusion tunes neuronal chloride homeostasis. Neuropharmacology 169, 107571. https://doi.org/10.1016/j.neuropharm.2019.03.014

Dallérac, G., Chever, O., Rouach, N., 2013. How do astrocytes shape synaptic transmission? Insights from electrophysiology. Front. Cell. Neurosci. 7. https://doi.org/10.3389/fncel.2013.00159

DeFazio, R.A., Keros, S., Quick, M.W., Hablitz, J.J., 2000. Potassium-Coupled Chloride Cotransport Controls Intracellular Chloride in Rat Neocortical Pyramidal Neurons. J. Neurosci. 20, 8069–8076. https://doi.org/10.1523/JNEUROSCI.20-21-08069.2000

Delpire, E., Baranczak, A., Waterson, A.G., Kim, K., Kett, N., Morrison, R.D., Scott Daniels, J., David Weaver, C., Lindsley, C.W., 2012. Further optimization of the K-Cl cotransporter KCC2 antagonist ML077: Development of a highly selective and more potent in vitro probe. Bioorg. Med. Chem. Lett. 22, 4532–4535. https://doi.org/10.1016/j.bmcl.2012.05.126

Djukic, B., Casper, K.B., Philpot, B.D., Chin, L.-S., McCarthy, K.D., 2007. Conditional Knock-Out of K_{ir} 4.1 Leads to Glial Membrane Depolarization, Inhibition of Potassium and Glutamate Uptake, and Enhanced Short-Term Synaptic Potentiation. J. Neurosci. 27, 11354–11365. https://doi.org/10.1523/JNEUROSCI.0723-07.2007

Düsterwald, K.M., Currin, C.B., Burman, R.J., Akerman, C.J., Kay, A.R., Raimondo, J.V., 2018. Biophysical models reveal the relative importance of transporter proteins and impermeant anions in chloride homeostasis. eLife 7, e39575. https://doi.org/10.7554/eLife.39575

Dzhala, V., Valeeva, G., Glykys, J., Khazipov, R., Staley, K., 2012. Traumatic Alterations in GABA Signaling Disrupt Hippocampal Network Activity in the Developing Brain. J. Neurosci. 32, 4017–4031. https://doi.org/10.1523/JNEUROSCI.5139-11.2012

Ferando, I., Faas, G.C., Mody, I., 2016. Diminished KCC2 confounds synapse specificity of LTP during senescence. Nat. Neurosci. 19, 1197–1200. https://doi.org/10.1038/nn.4357

Fiumelli, H., Briner, A., Puskarjov, M., Blaesse, P., Belem, B.J., Dayer, A.G., Kaila, K., Martin, J.-L., Vutskits, L., 2013. An Ion Transport-Independent Role for the Cation-Chloride Cotransporter KCC2 in Dendritic Spinogenesis In Vivo. Cereb. Cortex 23, 378–388. https://doi.org/10.1093/cercor/bhs027

Friedel, P., Kahle, K.T., Zhang, J., Hertz, N., Pisella, L.I., Buhler, E., Schaller, F., Duan, J., Khanna, A.R., Bishop, P.N., Shokat, K.M., Medina, I., 2015. WNK1-regulated inhibitory phosphorylation of the KCC2 cotransporter maintains the depolarizing action of GABA in immature neurons. Sci. Signal. 8. https://doi.org/10.1126/scisignal.aaa0354

Gagnon, M., Bergeron, M.J., Lavertu, G., Castonguay, A., Tripathy, S., Bonin, R.P., Perez-Sanchez, J., Boudreau, D., Wang, B., Dumas, L., Valade, I., Bachand, K., Jacob-Wagner, M., Tardif, C., Kianicka, I., Isenring, P., Attardo, G., Coull, J.A.M., De Koninck, Y., 2013. Chloride extrusion enhancers as novel therapeutics for neurological diseases. Nat. Med. 19, 1524–1528. https://doi.org/10.1038/nm.3356

Gauvain, G., Chamma, I., Chevy, Q., Cabezas, C., Irinopoulou, T., Bodrug, N., Carnaud, M., Lévi, S., Poncer, J.C., 2011. The neuronal K-Cl cotransporter KCC2 influences postsynaptic AMPA receptor content and lateral diffusion in dendritic spines. Proc. Natl. Acad. Sci. 108, 15474–15479. https://doi.org/10.1073/pnas.1107893108

Gavrilov, N., Golyagina, I., Brazhe, A., Scimemi, A., Turlapov, V., Semyanov, A., 2018. Astrocytic Coverage of Dendritic Spines, Dendritic Shafts, and Axonal Boutons in Hippocampal Neuropil. Front. Cell. Neurosci. 12, 248. https://doi.org/10.3389/fncel.2018.00248

Ge, W.-P., Duan, S., 2007. Persistent Enhancement of Neuron–Glia Signaling Mediated by Increased Extracellular K^+ Accompanying Long-Term Synaptic Potentiation. J. Neurophysiol. 97, 2564–2569. https://doi.org/10.1152/jn.00146.2006

Geiger, J.R.P., Jonas, P., 2000. Dynamic Control of Presynaptic Ca2+ Inflow by Fast-Inactivating K+ Channels in Hippocampal Mossy Fiber Boutons. Neuron 28, 927–939. https://doi.org/10.1016/S0896-6273(00)00164-1

Goutierre, M., Al Awabdh, S., Donneger, F., François, E., Gomez-Dominguez, D., Irinopoulou, T., Menendez De La Prida, L., Poncer, J.C., 2019. KCC2 Regulates Neuronal Excitability and Hippocampal Activity via Interaction with Task-3 Channels. Cell Rep. 28, 91-103.e7. https://doi.org/10.1016/j.celrep.2019.06.001

Grafstein, B., 1956. MECHANISM OF SPREADING CORTICAL DEPRESSION. J. Neurophysiol. 19, 154–171. https://doi.org/10.1152/jn.1956.19.2.154

Gulyás, A.I., Sík, A., Payne, J.A., Kaila, K., Freund, T.F., 2001. The KCl cotransporter, KCC2, is highly expressed in the vicinity of excitatory synapses in the rat hippocampus: Localization of KCC2 in the rat hippocampus. Eur. J. Neurosci. 13, 2205–2217. https://doi.org/10.1046/j.0953-816x.2001.01600.x

Harvey, C.D., Svoboda, K., 2007. Locally dynamic synaptic learning rules in pyramidal neuron dendrites. Nature 450, 1195–1200. https://doi.org/10.1038/nature06416

Hashimotodani, Y., Nasrallah, K., Jensen, K.R., Chávez, A.E., Carrera, D., Castillo, P.E., 2017. LTP at Hilar Mossy Cell-Dentate Granule Cell Synapses Modulates Dentate Gyrus Output by Increasing Excitation/Inhibition Balance. Neuron 95, 928-943.e3. https://doi.org/10.1016/j.neuron.2017.07.028

Henneberger, C., Bard, L., Panatier, A., Reynolds, J.P., Kopach, O., Medvedev, N.I., Minge, D., Herde, M.K., Anders, S., Kraev, I., Heller, J.P., Rama, S., Zheng, K., Jensen, T.P., Sanchez-Romero, I., Jackson, C.J., Janovjak, H., Ottersen, O.P., Nagelhus, E.A., Oliet, S.H.R., Stewart, M.G., Nägerl, U.V., Rusakov, D.A., 2020. LTP Induction Boosts Glutamate Spillover by Driving Withdrawal of Perisynaptic Astroglia. Neuron 108, 919-936.e11. https://doi.org/10.1016/j.neuron.2020.08.030

Henneberger, C., Papouin, T., Oliet, S.H.R., Rusakov, D.A., 2010. Long-term potentiation depends on release of d-serine from astrocytes. Nature 463, 232–236. https://doi.org/10.1038/nature08673

Henneberger, C., Rusakov, D.A., 2012. Monitoring local synaptic activity with astrocytic patch pipettes. Nat. Protoc. 7, 2171–2179. https://doi.org/10.1038/nprot.2012.140

Heubl, M., Zhang, J., Pressey, J.C., Al Awabdh, S., Renner, M., Gomez-Castro, F., Moutkine, I., Eugène, E., Russeau, M., Kahle, K.T., Poncer, J.C., Lévi, S., 2017. GABAA receptor dependent synaptic inhibition rapidly tunes KCC2 activity via the Cl−-sensitive WNK1 kinase. Nat. Commun. 8, 1776. https://doi.org/10.1038/s41467-017-01749-0

Hibino, H., Inanobe, A., Furutani, K., Murakami, S., Findlay, I., Kurachi, Y., 2010. Inwardly Rectifying Potassium Channels: Their Structure, Function, and Physiological Roles. Physiol. Rev. 90, 291–366. https://doi.org/10.1152/physrev.00021.2009

Higashi, K., Fujita, A., Inanobe, A., Tanemoto, M., Doi, K., Kubo, T., Kurachi, Y., 2001. An inwardly rectifying K^+ channel, Kir4.1, expressed in astrocytes surrounds synapses and blood vessels in brain. Am. J. Physiol.-Cell Physiol. 281, C922–C931. https://doi.org/10.1152/ajpcell.2001.281.3.C922

Hrabětová, S., Masri, D., Tao, L., Xiao, F., Nicholson, C., 2009. Calcium diffusion enhanced after cleavage of negatively charged components of brain extracellular matrix by chondroitinase ABC: Calcium diffusion enhanced after chondroitinase. J. Physiol. 587, 4029–4049. https://doi.org/10.1113/jphysiol.2009.170092

Hyde, T.M., Lipska, B.K., Ali, T., Mathew, S.V., Law, A.J., Metitiri, O.E., Straub, R.E., Ye, T., Colantuoni, C., Herman, M.M., Bigelow, L.B., Weinberger, D.R., Kleinman, J.E., 2011. Expression of GABA Signaling Molecules KCC2, NKCC1, and GAD1 in Cortical Development and Schizophrenia. J. Neurosci. 31, 11088–11095. https://doi.org/10.1523/JNEUROSCI.1234-11.2011

Ivakine, E.A., Acton, B.A., Mahadevan, V., Ormond, J., Tang, M., Pressey, J.C., Huang, M.Y., Ng, D., Delpire, E., Salter, M.W., Woodin, M.A., McInnes, R.R., 2013. Neto2 is a KCC2 interacting protein required for neuronal Cl^- regulation in hippocampal neurons. Proc. Natl. Acad. Sci. 110, 3561–3566. https://doi.org/10.1073/pnas.1212907110

Janach, G.M.S., Reetz, O., Döhne, N., Stadler, K., Grosser, S., Byvaltcev, E., Bräuer, A.U., Strauss, U., 2020. Interferon-γ acutely augments inhibition of neocortical layer 5 pyramidal neurons. J. Neuroinflammation 17, 69. https://doi.org/10.1186/s12974-020-1722-y

Jarolimek, W., Lewen, A., Misgeld, U., 1999. A Furosemide-Sensitive K^+–Cl^- Cotransporter Counteracts Intracellular Cl^- Accumulation and Depletion in Cultured Rat Midbrain

Neurons. J. Neurosci. 19, 4695–4704. https://doi.org/10.1523/JNEUROSCI.19-12-04695.1999

Kahle, K.T., Staley, K.J., Nahed, B.V., Gamba, G., Hebert, S.C., Lifton, R.P., Mount, D.B., 2008. Roles of the cation–chloride cotransporters in neurological disease. Nat. Clin. Pract. Neurol. 4, 490–503. https://doi.org/10.1038/ncpneuro0883

Kaila, K., Price, T.J., Payne, J.A., Puskarjov, M., Voipio, J., 2014. Cation-chloride cotransporters in neuronal development, plasticity and disease. Nat. Rev. Neurosci. 15, 637–654. https://doi.org/10.1038/nrn3819

Kakazu, Y., Uchida, S., Nakagawa, T., Akaike, N., Nabekura, J., 2000. Reversibility and Cation Selectivity of the K^+-Cl^- Cotransport in Rat Central Neurons. J. Neurophysiol. 84, 281–288. https://doi.org/10.1152/jn.2000.84.1.281

Kaupmann, K., Schuler, V., Mosbacher, J., Bischoff, S., Bittiger, H., Heid, J., Froestl, W., Leonhard, S., Pfaff, T., Karschin, A., Bettler, B., 1998. Human γ-aminobutyric acid type B receptors are differentially expressed and regulate inwardly rectifying K^+ channels. Proc. Natl. Acad. Sci. 95, 14991–14996. https://doi.org/10.1073/pnas.95.25.14991

Kirov, S.A., Sorra, K.E., Harris, K.M., 1999. Slices Have More Synapses than Perfusion-Fixed Hippocampus from both Young and Mature Rats. J. Neurosci. 19, 2876–2886. https://doi.org/10.1523/JNEUROSCI.19-08-02876.1999

Kofuji, P., Newman, E.A., 2004. Potassium buffering in the central nervous system. Neuroscience 129, 1043–1054. https://doi.org/10.1016/j.neuroscience.2004.06.008

Kurki, S.N., Srinivasan, R., Laine, J., Virtanen, M.A., Ala-Kurikka, T., Voipio, J., Kaila, K., 2023. Acute neuroinflammation leads to disruption of neuronal chloride regulation and consequent hyperexcitability in the dentate gyrus. Cell Rep. 42, 113379. https://doi.org/10.1016/j.celrep.2023.113379

Lee, H.H.C., Deeb, T.Z., Walker, J.A., Davies, P.A., Moss, S.J., 2011. NMDA receptor activity downregulates KCC2 resulting in depolarizing GABAA receptor–mediated currents. Nat. Neurosci. 14, 736–743. https://doi.org/10.1038/nn.2806

Li, H., Khirug, S., Cai, C., Ludwig, A., Blaesse, P., Kolikova, J., Afzalov, R., Coleman, S.K., Lauri, S., Airaksinen, M.S., Keinänen, K., Khiroug, L., Saarma, M., Kaila, K., Rivera, C., 2007. KCC2 Interacts with the Dendritic Cytoskeleton to Promote Spine Development. Neuron 56, 1019–1033. https://doi.org/10.1016/j.neuron.2007.10.039

Li, L., Chen, S.-R., Chen, H., Wen, L., Hittelman, W.N., Xie, J.-D., Pan, H.-L., 2016. Chloride Homeostasis Critically Regulates Synaptic NMDA Receptor Activity in Neuropathic Pain. Cell Rep. 15, 1376–1383. https://doi.org/10.1016/j.celrep.2016.04.039

Llano, O., Smirnov, S., Soni, S., Golubtsov, A., Guillemin, I., Hotulainen, P., Medina, I., Nothwang, H.G., Rivera, C., Ludwig, A., 2015. KCC2 regulates actin dynamics in

dendritic spines via interaction with β-PIX. J. Cell Biol. 209, 671–686. https://doi.org/10.1083/jcb.201411008

Loh, K.H., Stawski, P.S., Draycott, A.S., Udeshi, N.D., Lehrman, E.K., Wilton, D.K., Svinkina, T., Deerinck, T.J., Ellisman, M.H., Stevens, B., Carr, S.A., Ting, A.Y., 2016. Proteomic Analysis of Unbounded Cellular Compartments: Synaptic Clefts. Cell 166, 1295-1307.e21. https://doi.org/10.1016/j.cell.2016.07.041

Magloire, V., Cornford, J., Lieb, A., Kullmann, D.M., Pavlov, I., 2019. KCC2 overexpression prevents the paradoxical seizure-promoting action of somatic inhibition. Nat. Commun. 10, 1225. https://doi.org/10.1038/s41467-019-08933-4

Mahadevan, V., Woodin, M.A., 2016. Regulation of neuronal chloride homeostasis by neuromodulators: Neuromodulation of neuronal chloride homeostasis. J. Physiol. 594, 2593–2605. https://doi.org/10.1113/JP271593

Mapplebeck, J.C.S., Lorenzo, L.-E., Lee, K.Y., Gauthier, C., Muley, M.M., De Koninck, Y., Prescott, S.A., Salter, M.W., 2019. Chloride Dysregulation through Downregulation of KCC2 Mediates Neuropathic Pain in Both Sexes. Cell Rep. 28, 590-596.e4. https://doi.org/10.1016/j.celrep.2019.06.059

Medina, I., Friedel, P., Rivera, C., Kahle, K.T., Kourdougli, N., Uvarov, P., Pellegrino, C., 2014. Current view on the functional regulation of the neuronal K+-Cl− cotransporter KCC2. Front. Cell. Neurosci. 8. https://doi.org/10.3389/fncel.2014.00027

Meeks, J.P., Mennerick, S., 2007. Astrocyte membrane responses and potassium accumulation during neuronal activity. Hippocampus 17, 1100–1108. https://doi.org/10.1002/hipo.20344

Moore, Y.E., Kelley, M.R., Brandon, N.J., Deeb, T.Z., Moss, S.J., 2017. Seizing Control of KCC2: A New Therapeutic Target for Epilepsy. Trends Neurosci. 40, 555–571. https://doi.org/10.1016/j.tins.2017.06.008

Nakase, T., Naus, C.C.G., 2004. Gap junctions and neurological disorders of the central nervous system. Biochim. Biophys. Acta BBA - Biomembr. 1662, 149–158. https://doi.org/10.1016/j.bbamem.2004.01.009

Octeau, J.C., Chai, H., Jiang, R., Bonanno, S.L., Martin, K.C., Khakh, B.S., 2018. An Optical Neuron-Astrocyte Proximity Assay at Synaptic Distance Scales. Neuron 98, 49-66.e9. https://doi.org/10.1016/j.neuron.2018.03.003

Payne, J.A., 1997. Functional characterization of the neuronal-specific K-Cl cotransporter: implications for $[K^+]_o$ regulation. Am. J. Physiol.-Cell Physiol. 273, C1516–C1525. https://doi.org/10.1152/ajpcell.1997.273.5.C1516

Perez-Pinzon, M.A., Tao, L., Nicholson, C., 1995. Extracellular potassium, volume fraction, and tortuosity in rat hippocampal CA1, CA3, and cortical slices during ischemia. J. Neurophysiol. 74, 565–573. https://doi.org/10.1152/jn.1995.74.2.565

Poolos, N.P., Mauk, M.D., Kocsis, J.D., 1987. Activity-evoked increases in extracellular potassium modulate presynaptic excitability in the CA1 region of the hippocampus. J. Neurophysiol. 58, 404–416. https://doi.org/10.1152/jn.1987.58.2.404

Rahmati, N., Hoebeek, F.E., Peter, S., De Zeeuw, C.I., 2018. Chloride Homeostasis in Neurons With Special Emphasis on the Olivocerebellar System: Differential Roles for Transporters and Channels. Front. Cell. Neurosci. 12, 101. https://doi.org/10.3389/fncel.2018.00101

Rasmussen, R., Nicholas, E., Petersen, N.C., Dietz, A.G., Xu, Q., Sun, Q., Nedergaard, M., 2019. Cortex-wide Changes in Extracellular Potassium Ions Parallel Brain State Transitions in Awake Behaving Mice. Cell Rep. 28, 1182-1194.e4. https://doi.org/10.1016/j.celrep.2019.06.082

Reichenbach, A., Derouiche, A., Kirchhoff, F., 2010. Morphology and dynamics of perisynaptic glia. Brain Res. Rev. 63, 11–25. https://doi.org/10.1016/j.brainresrev.2010.02.003

Rinehart, J., Maksimova, Y.D., Tanis, J.E., Stone, K.L., Hodson, C.A., Zhang, J., Risinger, M., Pan, W., Wu, D., Colangelo, C.M., Forbush, B., Joiner, C.H., Gulcicek, E.E., Gallagher, P.G., Lifton, R.P., 2009. Sites of Regulated Phosphorylation that Control K-Cl Cotransporter Activity. Cell 138, 525–536. https://doi.org/10.1016/j.cell.2009.05.031

Rivera, C., Voipio, J., Payne, J.A., Ruusuvuori, E., Lahtinen, H., Lamsa, K., Pirvola, U., Saarma, M., Kaila, K., 1999. The K+/Cl− co-transporter KCC2 renders GABA hyperpolarizing during neuronal maturation. Nature 397, 251–255. https://doi.org/10.1038/16697

Rusakov, D.A., Kullmann, D.M., 1998. Extrasynaptic Glutamate Diffusion in the Hippocampus: Ultrastructural Constraints, Uptake, and Receptor Activation. J. Neurosci. 18, 3158–3170. https://doi.org/10.1523/JNEUROSCI.18-09-03158.1998

Saghyan, A., Lewis, D.P., Hrabe, J., Hrabetova, S., 2012. Extracellular diffusion in laminar brain structures exemplified by hippocampus. J. Neurosci. Methods 205, 110–118. https://doi.org/10.1016/j.jneumeth.2011.12.008

Shih, P.-Y., Savtchenko, L.P., Kamasawa, N., Dembitskaya, Y., McHugh, T.J., Rusakov, D.A., Shigemoto, R., Semyanov, A., 2013. Retrograde synaptic signaling mediated by K+ efflux through postsynaptic NMDA receptors. Cell Rep. 5, 941–951. https://doi.org/10.1016/j.celrep.2013.10.026

Sibille, J., Pannasch, U., Rouach, N., 2014. Astroglial potassium clearance contributes to short-term plasticity of synaptically evoked currents at the tripartite synapse: Astroglial currents and short-term plasticity. J. Physiol. 592, 87–102. https://doi.org/10.1113/jphysiol.2013.261735

Simard, C.F., Bergeron, M.J., Frenette-Cotton, R., Carpentier, G.A., Pelchat, M.-E., Caron, L., Isenring, P., 2007. Homooligomeric and Heterooligomeric Associations between K+-Cl– Cotransporter Isoforms and between K+-Cl– and Na+-K+-Cl– Cotransporters. J. Biol. Chem. 282, 18083–18093. https://doi.org/10.1074/jbc.M607811200

Sivakumaran, S., Cardarelli, R.A., Maguire, J., Kelley, M.R., Silayeva, L., Morrow, D.H., Mukherjee, J., Moore, Y.E., Mather, R.J., Duggan, M.E., Brandon, N.J., Dunlop, J., Zicha, S., Moss, S.J., Deeb, T.Z., 2015. Selective Inhibition of KCC2 Leads to Hyperexcitability and Epileptiform Discharges in Hippocampal Slices and *In Vivo*. J. Neurosci. 35, 8291–8296. https://doi.org/10.1523/JNEUROSCI.5205-14.2015

Sodickson, D.L., Bean, B.P., 1996. GABA $_B$ Receptor-Activated Inwardly Rectifying Potassium Current in Dissociated Hippocampal CA3 Neurons. J. Neurosci. 16, 6374–6385. https://doi.org/10.1523/JNEUROSCI.16-20-06374.1996

Somjen, G.G., 1979. Extracellular Potassium in the Mammalian Central Nervous System. Annu. Rev. Physiol. 41, 159–177. https://doi.org/10.1146/annurev.ph.41.030179.001111

Spoljaric, I., Spoljaric, A., Mavrovic, M., Seja, P., Puskarjov, M., Kaila, K., 2019. KCC2-Mediated Cl− Extrusion Modulates Spontaneous Hippocampal Network Events in Perinatal Rats and Mice. Cell Rep. 26, 1073-1081.e3. https://doi.org/10.1016/j.celrep.2019.01.011

Syková, E., Nicholson, C., 2008. Diffusion in Brain Extracellular Space. Physiol. Rev. 88, 1277–1340. https://doi.org/10.1152/physrev.00027.2007

Talifu, Z., Pan, Y., Gong, H., Xu, X., Zhang, C., Yang, D., Gao, F., Yu, Y., Du, L., Li, J., 2022. The role of KCC2 and NKCC1 in spinal cord injury: From physiology to pathology. Front. Physiol. 13, 1045520. https://doi.org/10.3389/fphys.2022.1045520

Thompson, S.M., Gahwiler, B.H., 1989. Activity-dependent disinhibition. II. Effects of extracellular potassium, furosemide, and membrane potential on ECl- in hippocampal CA3 neurons. J. Neurophysiol. 61, 512–523. https://doi.org/10.1152/jn.1989.61.3.512

Tyurikova, O., Shih, P.-Y., Dembitskaya, Y., Savtchenko, L.P., McHugh, T.J., Rusakov, D.A., Semyanov, A., 2022. K+ efflux through postsynaptic NMDA receptors suppresses local astrocytic glutamate uptake. Glia 70, 961–974. https://doi.org/10.1002/glia.24150

Uvarov, P., Ludwig, A., Markkanen, M., Pruunsild, P., Kaila, K., Delpire, E., Timmusk, T., Rivera, C., Airaksinen, M.S., 2007. A Novel N-terminal Isoform of the Neuron-specific K-Cl Cotransporter KCC2. J. Biol. Chem. 282, 30570–30576. https://doi.org/10.1074/jbc.M705095200

Uvarov, P., Ludwig, A., Markkanen, M., Soni, S., Hübner, C.A., Rivera, C., Airaksinen, M.S., 2009. Coexpression and Heteromerization of Two Neuronal K-Cl Cotransporter

Isoforms in Neonatal Brain. J. Biol. Chem. 284, 13696–13704. https://doi.org/10.1074/jbc.M807366200

Vargas-Caballero, M., Martin, L.J., Salter, M.W., Orser, B.A., Paulsen, O., 2010. α5 Subunit-containing GABAA receptors mediate a slowly decaying inhibitory synaptic current in CA1 pyramidal neurons following Schaffer collateral activation. Neuropharmacology 58, 668–675. https://doi.org/10.1016/j.neuropharm.2009.11.005

Verkhratsky, A., Nedergaard, M., 2018. Physiology of Astroglia. Physiol. Rev. 98, 239–389. https://doi.org/10.1152/physrev.00042.2016

Verselis, V.K., Srinivas, M., 2013. Connexin channel modulators and their mechanisms of action. Neuropharmacology 75, 517–524. https://doi.org/10.1016/j.neuropharm.2013.03.020

Viitanen, T., Ruusuvuori, E., Kaila, K., Voipio, J., 2010. The K^+–Cl^- cotransporter KCC2 promotes GABAergic excitation in the mature rat hippocampus. J. Physiol. 588, 1527–1540. https://doi.org/10.1113/jphysiol.2009.181826

Wallraff, A., Köhling, R., Heinemann, U., Theis, M., Willecke, K., Steinhäuser, C., 2006. The Impact of Astrocytic Gap Junctional Coupling on Potassium Buffering in the Hippocampus. J. Neurosci. 26, 5438–5447. https://doi.org/10.1523/JNEUROSCI.0037-06.2006

Wang, X., Lambert, N.A., 2000. $GABA_B$ Receptors Couple to Potassium and Calcium Channels on Identified Lateral Perforant Pathway Projection Neurons. J. Neurophysiol. 83, 1073–1078. https://doi.org/10.1152/jn.2000.83.2.1073

Weilinger, N.L., Wicki-Stordeur, L.E., Groten, C.J., LeDue, J.M., Kahle, K.T., MacVicar, B.A., 2022. KCC2 drives chloride microdomain formation in dendritic blebbing. Cell Rep. 41, 111556. https://doi.org/10.1016/j.celrep.2022.111556

Witcher, M.R., Kirov, S.A., Harris, K.M., 2007. Plasticity of perisynaptic astroglia during synaptogenesis in the mature rat hippocampus. Glia 55, 13–23. https://doi.org/10.1002/glia.20415

Wright, R., Newey, S.E., Ilie, A., Wefelmeyer, W., Raimondo, J.V., Ginham, R., Mcllhinney, R.A.J., Akerman, C.J., 2017. Neuronal Chloride Regulation via KCC2 Is Modulated through a $GABA_B$ Receptor Protein Complex. J. Neurosci. 37, 5447–5462. https://doi.org/10.1523/JNEUROSCI.2164-16.2017

Wu, Y.-W., Grebenyuk, S., McHugh, T.J., Rusakov, D.A., Semyanov, A., 2012. Backpropagating Action Potentials Enable Detection of Extrasynaptic Glutamate by NMDA Receptors. Cell Rep. 1, 495–505. https://doi.org/10.1016/j.celrep.2012.03.007

Yuste, R., Bonhoeffer, T., 2001. Morphological Changes in Dendritic Spines Associated with Long-Term Synaptic Plasticity. Annu. Rev. Neurosci. 24, 1071–1089. https://doi.org/10.1146/annurev.neuro.24.1.1071

Zhu, G., Liu, Y., Wang, Y., Bi, X., Baudry, M., 2015. Different Patterns of Electrical Activity Lead to Long-term Potentiation by Activating Different Intracellular Pathways. J. Neurosci. 35, 621–633. https://doi.org/10.1523/JNEUROSCI.2193-14.2015

List of publications

Byvaltcev, E., Behbood, M., Schleimer, J.-H., Gensch, T., Semyanov, A., Schreiber, S., Strauss, U., 2023. KCC2 reverse mode helps to clear postsynaptically released potassium at glutamatergic synapses. Cell Rep. 42, 112934. https://doi.org/10.1016/j.celrep.2023.112934

Döhne, N., Falck, A., Janach, G.M.S., **Byvaltcev, E.**, Strauss, U., 2022. Interferon-γ augments GABA release in the developing neocortex via nitric oxide synthase/soluble guanylate cyclase and constrains network activity. Front. Cell. Neurosci. 16, 913299. https://doi.org/10.3389/fncel.2022.913299

Janach, G.M.S., Reetz, O., Döhne, N., Stadler, K., Grosser, S., **Byvaltcev, E.**, Bräuer, A.U., Strauss, U., 2020. Interferon-γ acutely augments inhibition of neocortical layer 5 pyramidal neurons. J. Neuroinflammation 17, 69. https://doi.org/10.1186/s12974-020-1722-y